A Discrete Coupled Multiphase Interleaved LLC Converter With Symmetrical Components Analysis

Xiang Zhang, Shangzhi Pan, *Senior Member, IEEE*, and Praveen Jain, *Fellow, IEEE*

***Abstract*—This article proposes a coupling structure and a generalized analysis approach for multiphase interleaved *LLC* converters that applies to all odd phases that can simultaneously improve the current balancing in all interleaved phases. First, a discrete coupled inductor array (DCIArray) structure is proposed, and its magnetic circuit model is analyzed in detail; then, the generalized symmetrical component theory is introduced to decouple the inductance matrix to the sequence impedance, with expansion to all odd-phase *LLC* converters, and then, the sequence impedance, coupling coefficient, components tolerance impacts, and extended voltage gain with control architecture are discussed under the corresponding models; finally, the recommended design for three-phase and five-phase DCIArray was discussed. Experiments based on both three-phase and five-phase prototypes have proved that the proposed scheme has excellent current sharing in almost all frequency ranges.**

***Index Terms*—Coupled inductor, current balancing, interleaved, multiphase *LLC*, sequence impedance, symmetrical components theory.**

I. Introduction

HIGH-EFFICIENCY resonant dc–dc converters have now been widely accepted and applied in industrial and commercial fields, among them, the *LLC* converter is the most popular, thanks to its well-investigated electrical mechanism [11], [18], [39], practical control techniques [12], [15], [20], and possibility of integration in massive manufacturing [2], [19]. Therefore, it is not surprising that many researchers are pushing *LLC* converter to its limit, especially in high current demanding fields like modern telecom/ server, where paralleling and current balancing become a problem.

The origin of current unbalance comes from deviated voltage gain for different phases, as referred in [26], and a deeper reason is impedance unmatching, in other words, the tolerance of the components. Study in [32] has verified that only 5% resonant components tolerance could cause extreme power distribution uneven. This problem could be worse in parallel-input–parallel-output system, where variable frequency control is not a practical option to help the current sharing.

Manuscript received 31 January 2023; revised 21 April 2023; accepted 20 May 2023. Date of publication 25 May 2023; date of current version 22 September 2023. Recommended for publication by Associate Editor X. Pei. *(Corresponding author: Xiang Zhang.)*

Xiang Zhang and Praveen Jain are with the Department of Electrical and Computer Engineering, Queen's University, Kingston, ON K7L 3N6, Canada (e-mail: xiang.zhang@queensu.ca; praveen.jain@queensu.ca).

Shangzhi Pan is with the School of Electrical Engineering and Automation, Wuhan University, Wuhan 430072, China (e-mail: shangzhi.pan@whu.edu.cn).

Color versions of one or more figures in this article are available at https://doi.org/10.1109/TPEL.2023.3279822.

Digital Object Identifier 10.1109/TPEL.2023.3279822

To tackle the difficulty of unbalancing current in multiphase *LLC*, extensive method has been proposed. Modern current sharing techniques in multiphase *LLC* converters can be categorized into three types: control based, auxiliary circuit based, and topology based. Most studies start with a simple two-phase *LLC* converter module, to investigate the current balancing intrinsic, however, it is remarkable that some strategies have the potential to expand to multiphase and interleave scenarios, but some are not.

A. Control-Based Techniques

Pure control-based techniques are cost-friendly and accessible for all *LLC* converters as long as the calculation resources permit, among them the most feasible method is phase shifting. The main idea of phase shift balancing is using controllable unbalanced voltage excitation to adjust unbalanced current. The authors in [23] and [30], respectively, proposed methods of shifting the primary or secondary full bridges, by generating a duty cycle adjustable three-level voltage excitation at the primary or secondary side, to constrain the unbalancing current in two resonant tanks, this method is straightforward, but each module requires at least one full-bridge structure to make the three-level excitation possible; Arshadi et al. [4] take advantage of the natural current trigonometric principle of three-phase star connection *LLC*, by changing the lagging phase angle of the three phases voltage excitation to correct the unbalancing current.

B. Auxiliary Circuit-Based Techniques

It is a common application to use auxiliary circuit for current balancing, more flexible than other techniques but requires more hardware resources. From a different technical perspective, the balancing implementation is different.

One intuitive perspective is to control the resonant component value directly, thus the tolerance of the current sharing sensitive parameters are under control, for example, the authors in [16] and [17] insert a full-wave or half-wave switches-controlled capacitor (SCC) in each phase's resonant tank, so the equivalent resonant capacitor value in each phase is under control, and current sharing is not a problem; the similar idea can be applied to resonant inductors [27], [38], however, a controllable variable inductor is much harder to realize in hardware, usually it utilizes the saturation characteristic of the magnetics, which inevitable increases magnetic losses.

Starting with the perspective of partial energy processing, the auxiliary circuit can deal with the differential power directly, getting current in *LLC* modules back to even. Chen et al. [6] start from an auxiliary winding buck regulator at the rectification side; Wang et al. [37] start with an auxiliary winding dual-active bridge circuit at primary side, both fulfill the purpose of current sharing in *LLC* modules by partial energy processing. Apparently, these balancing techniques require consistent power monitoring and feedback calculation, and cannot be employed in open-loop systems.

C. Topology-Based Techniques

Topology-based techniques mainly refer to those methods that could take advantage of the native current balancing capability of topology, without introducing extra sampling, calculation, and control complexity, most of them could also work with the combination of other control techniques to have better behavior. They could be sorted into circuit topology dependent and magnetic topology dependent.

1) Circuit Topology Dependent: In circuit topology dependent, floating delta/star connection of the resonant capacitor at the primary side has been adopted in three-phase interleave *LLC* converters to reduce unbalance [13], [21], but they are only suitable for the interleaved three-phase system; while Wang et al. [35] used a *CLC* output filter to substitute the traditional bulk *C* filter to suppress the worst case unbalance current flow through the load, making the five-phase interleaved *LLC* balancing possible, whereas inevitable introduce more passive components. By sacrificing interleaving ability, the authors in [31] and [33] used a common shared inductor or capacitor as resonant components, and get a perfect current sharing, naming it passive impedance matching technique, they also give a detailed mathematical model to assess the balancing effect.

2) Magnetic Topology Dependent: For magnetic topology dependent, coupled inductor-based balancing techniques have got attention by the researchers, in [25], researchers found that a single balancing transformer could mitigate unbalanced current in a three-phase interleaved *LLC* converter; this idea was soon get verified by a four-phase *LLC* converters [1] with a similar balancing transformer called interleaved current balancing coupled inductor; another group used an inversely coupled inductors between three-phase *LLC* called multiphase inverse coupled resonant inductor (ICRI) [36], providing current sharing and extra leakage inductance for the converter. However, the aforementioned coupled techniques either have limitations in magnetics geometrical design or have shortages in interleaving operation, these weaknesses will be discussed comprehensively later in the content.

In fact, the idea of current sharing relying on a multiphase coupled inductor commonly exists for a "generalized *LLC* converter" as long as there exist sinusoidal like current flow through the primary side; the coupled inductor is always an option to balance the current. Guo et al. [14] have shown a multiparallel inverter with all phases synchronized, although the converter actually used a higher order resonant tank, rather than an *LLC* resonant tank, the current in the primary can still be balanced due to the coupled inductor.

Another magnetic topology-dependent method attached their attention to transformer coupling, since the extra output windings of one phase's transformer can be utilized as a controller factor in other phases, the multiphase *LLC* converter can be coupled by grouping the windings of each phase's transformer. If the grouping happens in the secondary windings using series connection like [40], the tolerance of each phase will be attenuated equivalently, with the cost of incapability of phase interleaving; if the grouping happens in the primary like [8], [9], then we can treat these extra windings as virtual controllable voltage sources, with the help of phase shift control, the current sharing can be obtained.

The main contributions of this article are as follows.

1) Proposed a magnetics coupling structure that inherently balances the current in the multiphase interleaved *LLC* converter, unlike traditional magnetic topology-based balancing techniques, this structure is free from the magnetics geometric shape, and the coupled inductor could be reutilized as resonant elements, with the possibility of integration in one core.
2) Proposed a generalized model using the symmetrical components theory, expanding the coupled magnetics application to all odd-phase interleaved *LLC* converters, providing an assessment method of the current balancing ability under sequence impedance.

II. Modeling and Symmetrical Component Analysis for the Discrete Coupled Multiphase Inductor

In this section, the reluctance and corresponding inductance-dual model of the three-phase DCIArray is derived based on the proposed coupling structure. Then, the symmetrical components theory is applied to evaluate the sequence impedance for this model, with an expansion to the multiphase circumstances. Furthermore, the influence of coupling coefficient and components tolerance are discussed for the current sharing benefit. Finally, a revised voltage gain characteristic of the proposed converter is discussed with a feasible variable frequency control architecture.

A. Magnetic Model Derivation

Fig. 1(c) has shown the proposed schematic of a three-phase discrete coupled *LLC* converter, as well as the winding structure of a three-phase DCIArray. To demonstrate this structure mathematically, a reluctance model is used in Fig. 2. There are three independent inductors L_{b1}, L_{b2}, and L_{b3} with the same core size and the same air gap at the center leg, all windings are tangling around the center leg, when each independent inductor includes all different phasor's winding, it is call "full stack," otherwise it is "nonfull stack." Naming the center leg reluctances as $\mathcal{R}_{b1}$, $\mathcal{R}_{b2}$, $\mathcal{R}_{b3}$, and the leakage reluctance as $\mathcal{R}_{\mathrm{lk}}$.

The balancing nature relies on the winding arrangements: for each phase, the total winding turns should equal; for each inductor, the total winding turns should also equal; in other words, the winding structure for three phases should be absolutely symmetrical. Therefore, the winding turns numbers

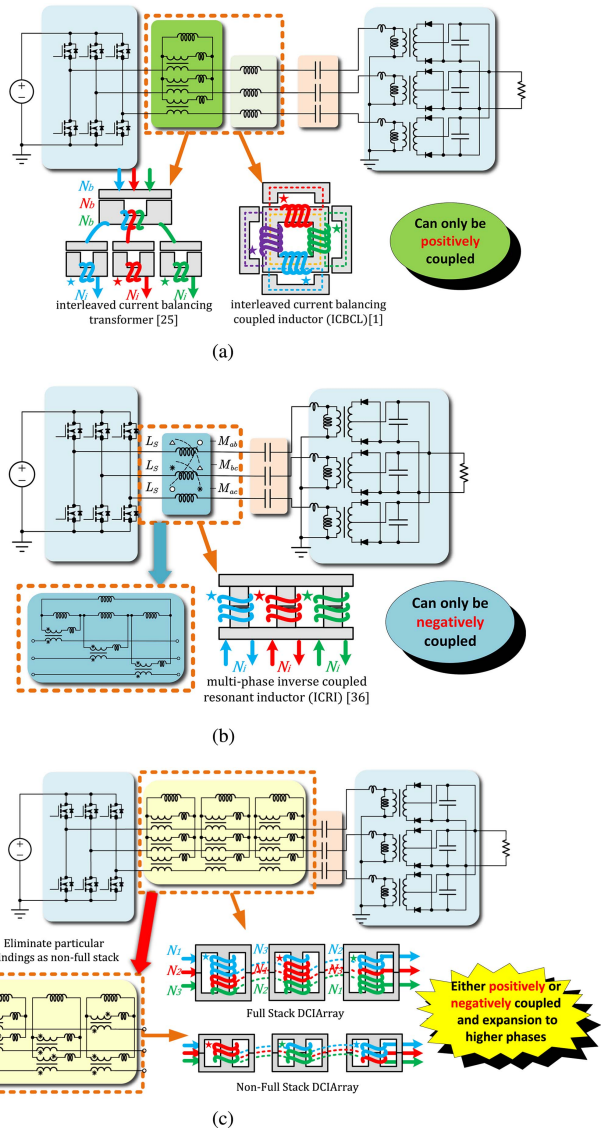

Fig. 1. Latest magnetic-based coupling structure for the interleaved *LLC*. (a) Three-phase *LLC* converter with a single balancing transformer (inductor) in [1] and [25]. (b) Three-phase *LLC* converter with a single inversely coupled multileg inductor in [36]. (c) Proposed three-phase *LLC* with three discrete coupled inductor.

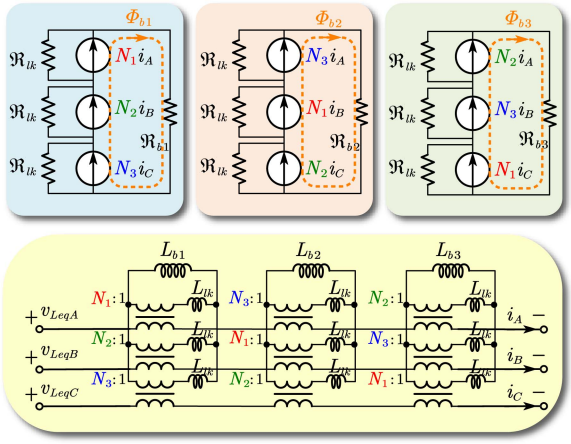

Fig. 2. Reluctance and inductance dual model for the three-phase DCIArray.

and arrangement order for each inductor is fixed, represented as N_1, N_2, N_3 on L_{b1}, N_3, N_1, N_2 on L_{b2}, and N_2, N_3, N_1 on L_{b3}. Magnetomotive force (MMF) sources detailed this coil connection method in this reluctance model.

Due to the high reluctance path of leakage flux and low coil turns in practical coupled inductor design, the leakage flux for each coupled inductor could be ignored, thus the flux flow through each center leg can be considered as a direct collaborative effect of the three-phase MMF source. Then, we can derive the magnetic flux equation as

$$\begin{cases} \Phi_{b1} = \frac{(N_1 i_a + N_2 i_b + N_3 i_c)}{\mathcal{R}_{b1}} \\ \Phi_{b2} = \frac{(N_3 i_a + N_1 i_b + N_2 i_c)}{\mathcal{R}_{b2}} \\ \Phi_{b3} = \frac{(N_2 i_a + N_3 i_b + N_1 i_c)}{\mathcal{R}_{b3}}. \end{cases} \tag{1}$$

Apparently, the coupled inductor magnetic flux does not need to be zero since the coil turns N_1, N_2, and N_3 can be any integer value. The essence of reutilizing coupled inductors as resonant components are to make full use of this nonzero magnetic flux.

It is worth noting a topological equivalent inductance dual model [7] of the proposed reluctance model, which was shown in Fig. 2. From the view of the multiwinding transformer, the coupled inductor can be treated as a balancing transformer group. This model is very conducive for manufacture measurement and computer-aided simulation, since both the magnetizing and leakage inductance value for each coupled inductor element can be easily obtained by an *LCR* meter, and the ideal transformer and ideal inductor are available in almost every simulation software. Besides, this approach also gives insight into simplifying the inductance matrix as we will show in the following content.

Following the simplification methodology of omitting the leakage elements, the total equivalent voltage across each phase in the DCIArray can be obtained by Faraday's law, expressed as

$$\begin{cases} v_{Leqa} = N_1 \frac{d\Phi_{b1}}{dt} + N_3 \frac{d\Phi_{b2}}{dt} + N_2 \frac{d\Phi_{b3}}{dt} \\ v_{Leqb} = N_2 \frac{d\Phi_{b1}}{dt} + N_1 \frac{d\Phi_{b2}}{dt} + N_3 \frac{d\Phi_{b3}}{dt} \\ v_{Leqc} = N_3 \frac{d\Phi_{b1}}{dt} + N_2 \frac{d\Phi_{b2}}{dt} + N_1 \frac{d\Phi_{b3}}{dt} \end{cases} \tag{2}$$

where v_{Leqa}, v_{Leqb}, and v_{Leqc} are the total equivalent voltage for phases A, B, and C, respectively. Then, we can substitute the magnetic flux equation into (1) to get the inductance matrix of the reluctance model, then we have For abbreviation purposes, we denote the inductance matrix elements as self-inductance and mutual inductance in (3) shown at the bottom of next page. L_{sa}, L_{sb}, and L_{sc} are the self-inductance for each phase; and M_{ab}, M_{bc}, and M_{ac} are the mutual inductance between phases A and B, B and C, and A and C, respectively. The whole coupled inductance matrix is marked as $\mathbf{Z_{abc}}$, then (3) can be simplified as

$$\begin{bmatrix} v_{Leqa} \\ v_{Leqb} \\ v_{Leqc} \end{bmatrix} = \begin{bmatrix} L_{sa} & M_{ab} & M_{ac} \\ M_{ab} & L_{sb} & M_{bc} \\ M_{ac} & M_{bc} & L_{sc} \end{bmatrix} \begin{bmatrix} \frac{di_a}{dt} \\ \frac{di_b}{dt} \\ \frac{di_c}{dt} \end{bmatrix} = \mathbf{Z_{abc}} \begin{bmatrix} \frac{di_a}{dt} \\ \frac{di_b}{dt} \\ \frac{di_c}{dt} \end{bmatrix}. \tag{4}$$

If it is possible to perfectly control the tolerance of reluctance on each inductor, assuming $\mathcal{R}_{b1} = \mathcal{R}_{b2} = \mathcal{R}_{b3} = \mathcal{R}_b = 1/L_b$, then the self-inductance and mutual inductance values will be related with winding turns and single turn inductance L_b only, this assumption can be taken down as

$$\begin{cases} L_{sa} = L_{sb} = L_{sc} = L_s = \left(N_1^2 + N_2^2 + N_3^2\right) L_b \\ M_{ab} = M_{ac} = M_{bc} = L_m = (N_2N_1 + N_2N_3 + N_3N_1)L_b. \end{cases} \tag{5}$$

When the assumption does not meet, the tolerance of each discrete inductor will weaken the balancing behavior, which will be discussed in Section II-D.

B. Symmetrical Components Analyze

The symmetrical component theory has been well investigated and widely applied to the analysis of power system unsymmetrical operation, imbalance fault of synchronous motors [3], and voltage rebalance of STATCOM [5]. However, there are rare topics concerning symmetrical theory application in high-frequency multiphase resonant converters, even though *LLC* converters perform perfect sinusoidal behavior. In this article, the symmetrical component theory is utilized, combined with the fundamental harmonics approximation (FHA) method, to describe the balancing nature of the multiphase discrete coupled interleaved *LLC* converter in the perspective of sequence impedance. We first begin with a three-phase system.

In a steady-state three-phase circuit, any group of asymmetric three-phase phasors (current or voltage) can be decomposed into three groups of symmetrical components. When phase A is selected as the reference phase, this relationship (take phase voltage as an example)

$$\begin{bmatrix} V_{sc\_0} \\ V_{sc\_1} \\ V_{sc\_2} \end{bmatrix} = \frac{1}{3} \begin{bmatrix} 1 & 1 & 1 \\ 1 & \alpha^1 & \alpha^2 \\ 1 & \alpha^2 & \alpha^1 \end{bmatrix} \begin{bmatrix} V_a \\ V_b \\ V_c \end{bmatrix} = \mathbf{S} \begin{bmatrix} V_a \\ V_b \\ V_c \end{bmatrix} \tag{6}$$

where α in the transformation matrix $\mathbf{S}$ equals to $e^{j2\pi/3}$, and I_{sc_0}, I_{sc_1}, and I_{sc_2} are defined as the current phasors of zero-, positive-, negative-sequence components, respectively. These phase sequences can be depicted in the phasor diagram in Fig. 3.

Clearly, when the symmetric components of each sequence are known, the inverse transformation can also be used to obtain the three-phase asymmetric phasor (take current as an example), namely

$$\begin{bmatrix} I_a \\ I_b \\ I_c \end{bmatrix} = \mathbf{S^{-1}} \begin{bmatrix} I_{sc\_0} \\ I_{sc\_1} \\ I_{sc\_2} \end{bmatrix} = \begin{bmatrix} 1 & 1 & 1 \\ 1 & \alpha^2 & \alpha^1 \\ 1 & \alpha^1 & \alpha^2 \end{bmatrix} \begin{bmatrix} I_{sc\_0} \\ I_{sc\_1} \\ I_{s\_2} \end{bmatrix}. \tag{7}$$

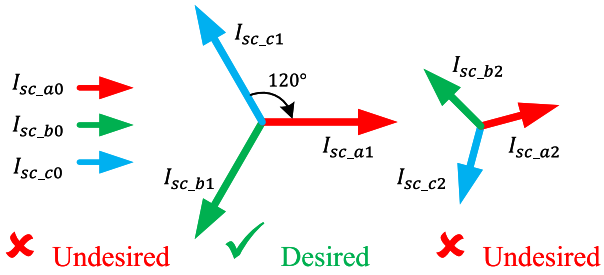

Fig. 3. Current phasors in three-phase *LLC*.

Then, we can substitute the total equivalent voltage across the inductor by symmetrical components into (4) as

$$\begin{aligned} \begin{bmatrix} v_{Leq0} \\ v_{Leq1} \\ v_{Leq2} \end{bmatrix} &= \mathbf{S} \begin{bmatrix} v_{Leqa} \\ v_{Leqb} \\ v_{Leqc} \end{bmatrix} = \mathbf{SZ_{abc}} \begin{bmatrix} \frac{di_a}{dt} \\ \frac{di_b}{dt} \\ \frac{di_c}{dt} \end{bmatrix} \\ &= \mathbf{SZ_{abc}S^{-1}} \begin{bmatrix} I_{Sc\_0} \\ I_{Sc\_1} \\ I_{sc\_2} \end{bmatrix} = \mathbf{Z_{012}} \begin{bmatrix} I_{sc\_0} \\ I_{sc\_1} \\ I_{sc\_2} \end{bmatrix} \end{aligned} \tag{8}$$

where $\mathbf{Z_{012}}$ is the sequence impedance matrix to the corresponding coupled inductance matrix $\mathbf{Z_{abc}}$.

Here, we first presume (8) satisfies the assumption condition in (5) for a decoupling analysis, then we will look deeper into the circumstances when the condition does not meet

$$\begin{aligned} \mathbf{Z_{012}} &= \begin{bmatrix} L_s + 2L_m & 0 & 0 \\ 0 & L_s - L_m & 0 \\ 0 & 0 & L_s - L_m \end{bmatrix} \\ &= \operatorname{diag}\left[L_{\text{eq0}}, L_{\text{eq1}}, L_{\text{eq2}}\right] \end{aligned} \tag{9}$$

where

$$\begin{cases} L_{\text{eq0}} = (N_1 + N_2 + N_3)^2 L_b \\ L_{\text{eq1}} = L_{\text{eq2}} \\ = \left[N_1^2 + N_2^2 + N_3^2 - (N_2N_1 + N_2N_3 + N_3N_1)\right] L_b. \end{cases} \tag{10}$$

When the reluctance on each inductor is identical, $\mathbf{Z_{012}}$ will degenerate into a pure diagonal array, making decoupling analysis for symmetrical components possible.

From the Cauchy–Schwarz inequality, we know that

$$\begin{aligned} &(N_1 + N_2 + N_3)^2 L_b \\ &\geq \left[N_1^2 + N_2^2 + N_3^2 - (N_2N_1 + N_2N_3 + N_3N_1)\right] L_b \geq 0. \end{aligned} \tag{11}$$

$$\begin{bmatrix} v_{Leqa} \\ v_{Leqb} \\ v_{Leqc} \end{bmatrix} = \begin{bmatrix} \left(\frac{N_1^2}{\mathcal{R}_{b1}} + \frac{N_3^2}{\mathcal{R}_{b2}} + \frac{N_2^2}{\mathcal{R}_{b3}}\right) & \left(\frac{N_1N_2}{\mathcal{R}_{b1}} + \frac{N_3N_1}{\mathcal{R}_{b2}} + \frac{N_2N_3}{\mathcal{R}_{b3}}\right) & \left(\frac{N_1N_3}{\mathcal{R}_{b1}} + \frac{N_3N_2}{\mathcal{R}_{b2}} + \frac{N_2N_1}{\mathcal{R}_{b3}}\right) \\ \left(\frac{N_1N_2}{\mathcal{R}_{b1}} + \frac{N_3N_1}{\mathcal{R}_{b2}} + \frac{N_2N_3}{\mathcal{R}_{b3}}\right) & \left(\frac{N_2^2}{\mathcal{R}_{b1}} + \frac{N_1^2}{\mathcal{R}_{b2}} + \frac{N_3^2}{\mathcal{R}_{b3}}\right) & \left(\frac{N_2N_3}{\mathcal{R}_{b1}} + \frac{N_2N_1}{\mathcal{R}_{b2}} + \frac{N_3N_1}{\mathcal{R}_{b3}}\right) \\ \left(\frac{N_1N_3}{\mathcal{R}_{b1}} + \frac{N_3N_2}{\mathcal{R}_{b2}} + \frac{N_2N_1}{\mathcal{R}_{b3}}\right) & \left(\frac{N_2N_3}{\mathcal{R}_{b1}} + \frac{N_2N_1}{\mathcal{R}_{b2}} + \frac{N_3N_1}{\mathcal{R}_{b3}}\right) & \left(\frac{N_3^2}{\mathcal{R}_{b1}} + \frac{N_2^2}{\mathcal{R}_{b2}} + \frac{N_1^2}{\mathcal{R}_{b3}}\right) \end{bmatrix} \begin{bmatrix} \frac{di_a}{dt} \\ \frac{di_b}{dt} \\ \frac{di_c}{dt} \end{bmatrix}. \tag{3}$$

The first equality is obtained only when $N_1 = N_2 = N_3 = 0$, which can never be achieved because each inductor should contain at least one turn; while the second equality is valid only when $N_1 = N_2 = N_3$.

The sequence current is related to sequence impedance, the high sequence impedance will suppress the corresponding sequence current. Therefore, it is obvious that the zero-sequence inductance L_{eq0} has a much higher value than positive- and negative-sequence inductance (L_{eq1}, L_{eq2}). We can have a basic understanding of how the zero-sequence current in three-phase *LLC* was suppressed thanks to this coupled structure.

C. Generalized Discrete Coupled Multiphase Inductor Structure

In the previous section, three-phase discrete coupled *LLC* is discussed from the perspective of sequence impedance, where unbalanced phase currents are decomposed to three groups of symmetrical current phasor, and different sequence currents will encounter different sequence impedance. This methodology can also be expanded to a multiphase system, by introducing the generalized symmetrical component theory [22].

In this theory, we assume that the converter has a total of m phases, where I_k is the current of the kth phase, similarly, there will be m symmetrical components, let I_{sc_k} be the corresponding kth sequence component current. Then, the transformation matrix can be expressed as $\mathbf{S}$ in (12) shown at the bottom of this page, where $\mathbf{a}$ equals to $e^{j2\pi/m}$ Then, a familiar transformation as (8) will help us to transform the original inductance matrix $\mathbf{Z_m}$ to the sequence impedance matrix $\mathbf{Z_{sc}}$ as follows:

$$\mathbf{Z_{sc}} = \mathbf{S}\mathbf{Z_m}\mathbf{S^{-1}} \tag{13}$$

$$\mathbf{Z_m} = \begin{bmatrix} L_{s1} & M_{12} & M_{13} & \cdots & M_{1\text{m}} \\ M_{12} & L_{s2} & M_{23} & \cdots & M_{2\text{m}} \\ M_{13} & M_{23} & L_{s3} & \cdots & M_{3\text{m}} \\ \vdots & \vdots & \vdots & \ddots & \vdots \\ M_{1\text{m}} & M_{2\text{m}} & M_{3\text{m}} & \cdots & L_{s\text{m}} \end{bmatrix}. \tag{14}$$

Following the same simplification process in the previous section, if the reluctance assumption of $\mathcal{R}_{b1} = \mathcal{R}_{b2} = \cdots = \mathcal{R}_{bm} = \mathcal{R}_b = 1/L_b$ remain valid, the inductance matrix $\mathbf{Z_m}$ is a real symmetrical matrix. Then, the elements in the inductance matrix $\mathbf{Z_m}$ can be written as

$$\begin{cases} L_{s1} = L_{s2} = \cdots = L_{sm} = \left(\sum_{i=1}^{m} N_i^2\right) L_b \\ M_{ij} = \left(\sum N_p N_q\right) L_b \\ (p, q \text{ are clockwise interval } |i-j|, \\ \qquad e.g.\ N_1 N_{(1+|i-j|)}, N_m N_{|i-j|}). \end{cases} \tag{15}$$

And the symmetrical component transformation will be a diagonalization process, the sequence impedance matrix could still keep the diagonal form after the transformation.

$$\begin{aligned} \mathbf{Z_{sc}} &= \begin{bmatrix} L_{\text{eq0}} & 0 & 0 & \cdots & 0 \\ 0 & L_{\text{eq1}} & 0 & \cdots & 0 \\ 0 & 0 & L_{\text{eq2}} & \cdots & 0 \\ \vdots & \vdots & \vdots & \ddots & \vdots \\ 0 & 0 & 0 & \cdots & L_{\text{eq}(m-1)} \end{bmatrix} \\ &= \text{diag}\left[L_{\text{eq0}}, L_{\text{eq1}}, L_{\text{eq2}}, \ldots, L_{\text{eq}(m-1)}\right]. \end{aligned} \tag{16}$$

One thing should be noted in the sequence impedance matrix $\mathbf{Z_{sc}}$ is the parity of phase number m; for the odd-phase coupled inductor, the symmetrical component transformation will deduce a single zero-sequence impedance L_{eq0} and a series of positive- and negative-sequence impedance in pair; for the even-phase coupled inductor, the transformation will give two zero-sequence impedances L_{eq0} and $L_{\text{eq}(m/2)}$, with the same positive- and negative-sequence impedance pair. This symmetrical impedance relationship can be depicted in Fig. 4(a).

For the even phases system, phase current can be decomposed into two groups of odd phases current that balances with each other. Since the current balance between these two groups is relatively complicated, it is not the focus of this article. Therefore, the following articles only discuss the case where m is an odd number.

Then, we can obtained the diagonal elements in $\mathbf{Z_{sc}}$ by combining (13)–(16) together, shown as follows:

$$\begin{cases} L_{\text{eq0}} = \left(\sum_{i=1}^{m} N_i\right)^2 L_b \\ L_{\text{eq}k} = L_{\text{eq}(m-k)} \\ = \left[\sum_{i=1}^{m} N_i^2 + 2\cos\left(k \cdot 1 \cdot \frac{2\pi}{m}\right) M_1 + 2\cos\left(k \cdot 2 \cdot \frac{2\pi}{m}\right) M_2 \right. \\ \left. + \cdots + 2\cos\left(k \cdot \frac{m-1}{2} \cdot \frac{2\pi}{m}\right) M_{\frac{m-1}{2}}^2\right] L_b (1 \le k \le m) \\ M_k = \sum N_i N_j \\ \left(i, j \text{ are clockwise interval } k, e.g., N_1 N_{(1+k)}, N_m N_k\right). \end{cases} \tag{17}$$

$$\begin{bmatrix} \boldsymbol{I}_{\text{sc\_}0} \\ \boldsymbol{I}_{\text{sc\_}1} \\ \boldsymbol{I}_{\text{sc\_}2} \\ \boldsymbol{I}_{\text{sc\_}3} \\ \vdots \\ \boldsymbol{I}_{\text{sc\_}k} \\ \vdots \\ \boldsymbol{I}_{\text{sc}(m-1)} \end{bmatrix} = \frac{1}{m} \bullet \begin{bmatrix} \mathbf{a}^0 & \mathbf{a}^0 & \mathbf{a}^0 & \cdots & \mathbf{a}^0 \\ \mathbf{a}^0 & \mathbf{a}^{1\cdot1} & \mathbf{a}^{2\cdot1} & \cdots & \mathbf{a}^{(m-1)\cdot1} \\ \mathbf{a}^0 & \mathbf{a}^{1\cdot2} & \mathbf{a}^{2\cdot2} & \cdots & \mathbf{a}^{(m-1)\cdot2} \\ \mathbf{a}^0 & \mathbf{a}^{1\cdot3} & \mathbf{a}^{2\cdot3} & \cdots & \mathbf{a}^{(m-1)\cdot3} \\ \vdots & \vdots & \vdots & \cdots & \vdots \\ \mathbf{a}^0 & \mathbf{a}^{1\cdot(k-1)} & \mathbf{a}^{2\cdot(k-1)} & \cdots & \mathbf{a}^{(k-1)\cdot(k-1)} \\ \vdots & \vdots & \vdots & \cdots & \vdots \\ \mathbf{a}^0 & \mathbf{a}^{1\cdot(m-1)} & \mathbf{a}^{2\cdot(m-1)} & \cdots & \mathbf{a}^{(m-1)\cdot(m-1)} \end{bmatrix} \begin{bmatrix} \boldsymbol{I}_1 \\ \boldsymbol{I}_2 \\ \boldsymbol{I}_3 \\ \boldsymbol{I}_4 \\ \vdots \\ \tilde{\boldsymbol{I}}_k \\ \vdots \\ \tilde{\boldsymbol{I}}_m \end{bmatrix} = \mathbf{S} \begin{bmatrix} \boldsymbol{I}_1 \\ \boldsymbol{I}_2 \\ \boldsymbol{I}_3 \\ \boldsymbol{I}_4 \\ \vdots \\ \tilde{\boldsymbol{I}}_k \\ \vdots \\ \tilde{\boldsymbol{I}}_m \end{bmatrix}. \tag{12}$$

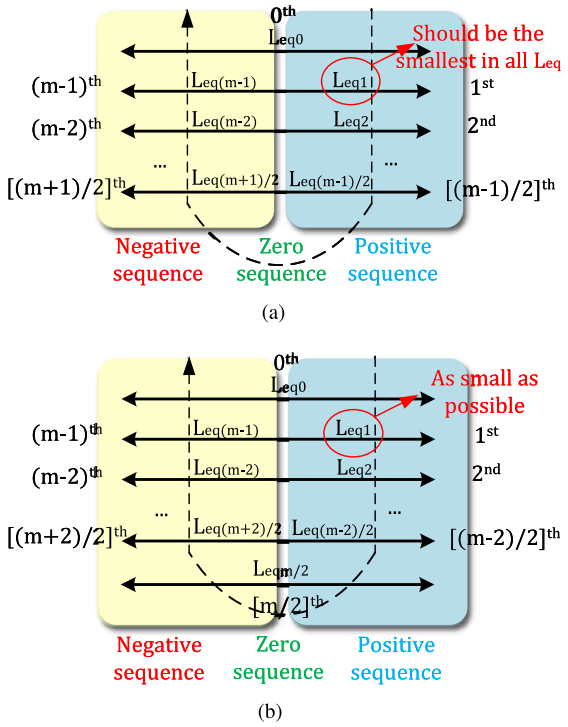

Fig. 4. Relationship of different sequence impedance. (a) Odd phases system. (b) Even phases system.

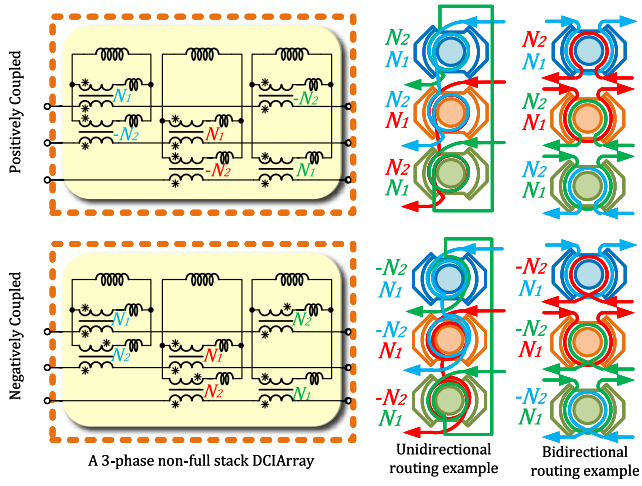

Fig. 5. Three-phase nonfull-stack DCIArray positive \ negative coupling structure with routing example.

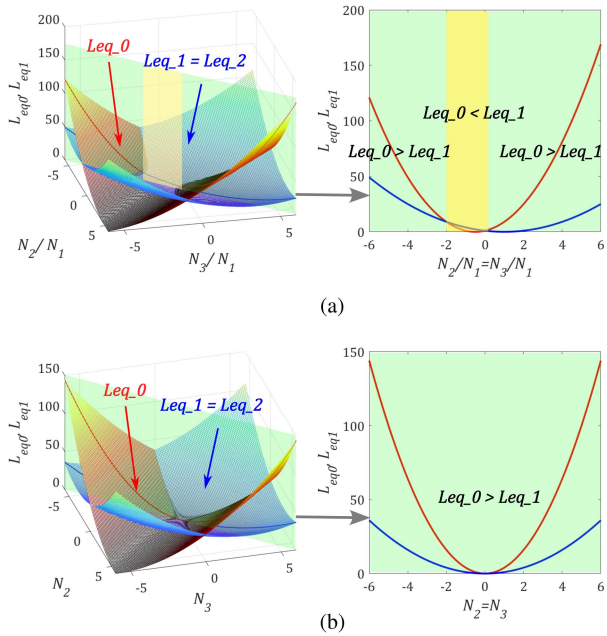

Fig. 6. Sequence impedance diagram for three-phase *LLC*. (a) Full-stack case. (b) Nonfull-stack case.

The aforementioned equation discloses that the DCIArray introduces a series of distinguishable positive- and negative-sequence impedance to the system, among them only the first sequence impedance L_{eq1} is responsible for the power delivery in the multiphase converter; and zero-sequence impedance L_{eq0} is larger than L_{eq1} and works as unbalancing factors. Therefore, undesired current components can be drifted away from the resonant point by properly designing the winding turns of discrete inductors, in other words, some particular combination of sequence impedance can suppress the undesired unbalanced sequence current. This process will be similar to the filter design, while the DCIArray performs like an unbalance current filter, letting the balance current flow through the filter and block off the unbalance current.

The generalized model also inspected the nonfull-stack DCIArray and negative coupled DCIArray. Comparing two different nonfull-stack coupling structures in Fig. 5, we can simply change the sign of N_2, and make N_3 to be zero, then either positively or negatively coupled inductor can be explained in the same mathematical form. In this scenario, zero $N_1, N_2, \ldots, N_m$ means that the corresponding phases are ruled out of coupling; while negative N_1, N_2, $\ldots$, N_m means that the inductors are inversely coupled. As long as these coupled inductors maintain the principle of symmetrical arrangements, the current balancing ability of the coupled magnetics can still be kept.

For better understanding, the relation of different sequence impedance, a graphical method can be utilized for impedance design. Fig. 6(a) is a example of three-phase full-stack DCIArray impedance diagram, with N_2/N_1 and N_3/N_1 as the variables, while Fig. 6(b) is the nonfull-stack impedance diagram, with N_2 and N_3 as the variables.

The sequence impedance diagram suggested that no matter the DCIArray is full stack or not, the changing trend of the sequence impedance will perform similarly as a large turns ratio is applied, the only difference is in neighborhoods of 1. If we draw a diagonal slice plane on $N_2 = N_3$, then this minor difference can be observed. In the full-stack case, it is possible to have zero L_{eq1} and positive L_{eq0} simultaneously (when $N_2 = N_3 = N_1$); while in the nonfull-stack case, there is only the existence of $L_{\text{eq0}} < L_{\text{eq1}}$ (positively coupled) or $L_{\text{eq0}} > L_{\text{eq1}}$ (negative coupled). This character can also be verified from the perspective of the coupling coefficient, the point of 1 is a special case of full-stack coupled DCIArray, with the system degeneration to a full positive coupling manner as mentioned in [24] and [25].

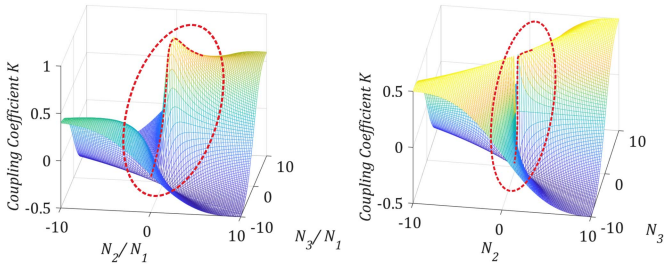

Fig. 7. Coupling coefficient for three-phase DCIArray full stack (left) and nonfull stack (right).

D. Coupling Coefficient and Tolerance Analysis

Looking back to a practical discrete coupled multiphase coupled *LLC* converter, the impacts of the resonant components' tolerance cannot be ignored. These components include leakage inductor, resonant capacitor, magnetizing inductor, and the reluctance of DCIArray (or unit inductor L_b). Since an analytic expression between current sharing and tolerances is nearly impossible to get, a numerical simulation based on the coupling coefficient can be considered as a tool to find out the tolerance impact on current balancing.

The general coupling coefficient can be calculated by (18), which implied that the coupling coefficient of DCIArray is only related to its winding turns.

$$K_{ij} = \frac{M_{ij}}{\sqrt{L_{si}L_{sj}}} = \frac{\sum N_p N_q}{\sum_{i=1}^{m} N_i^2} = \frac{\sum N_p N_q}{\sum_{i=1}^{m} N_i^2} = K_{|i-j|}$$
$$(p, q \text{ are clockwise interval } |i-j|,$$
$$e.g.\ N_1 N_{(1+|i-j|)}, N_m N_{|i-j|}) \tag{18}$$

where M_{ij} is the mutual-inductance between phase i and phase j, and L_i and L_j is the self-inductance of phase i and phase j, respectively. Review the mutual operator in (17), the coupling coefficient has a very similar form to M_k, in fact once the value of $|i-j|$ is the same, the corresponding coupling coefficient will be identical.

Therefore, for the three-phase system, there will be only one coupling coefficient, expressed as (19). Similarly, there will be full-stack case and nonfull-stack case of coupling coefficient diagram to plot, as depicted in Fig. 7.

$$K_{12} = K_{13} = K_{23} = \frac{N_1N_2 + N_1N_3 + N_2N_3}{N_1^2 + N_2^2 + N_3^2} = K. \tag{19}$$

For the full-stack case, the coupling coefficient ranges from -0.5 to 1, while in the nonfull-stack case, the ranges shrink to $-0.5 \sim 0.5$. Information from Fig. 7 suggests that coupling coefficient will change dramatically within the range of 0–5, and ± 0.5 of coupling coefficient is easy to obtain once the $N_1 = \pm N_2$, so it is unnecessary to have a large turns ratio when designing the DCIArray.

Now, a load current sharing error δ can be defined to demonstrate and compare the unbalanced behavior of the converter based on each phase's output current rms value, expressed as

$$\delta = \frac{\max\{I_1, I_2 \ldots I_m\} - \min\{I_1, I_2 \ldots I_m\}}{\sum_{i=1}^{m} I_i}. \tag{20}$$

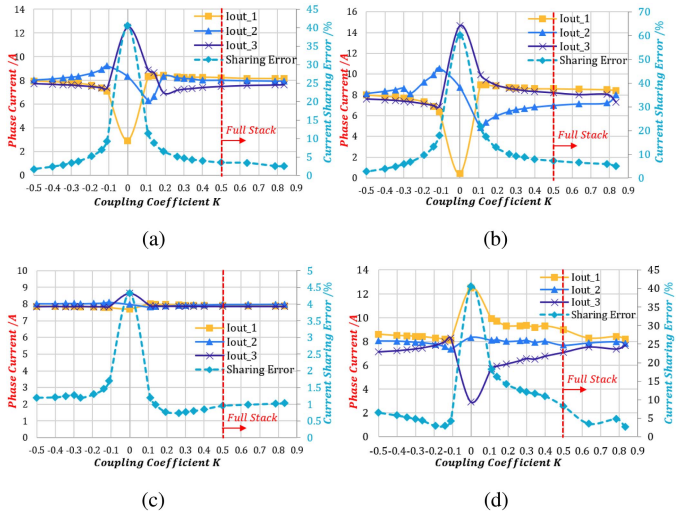

Fig. 8. Three-phase *LLC* current sharing error with components tolerance. (a) With $\pm 10\% L_r$ tolerance. (b) With $\pm 10\% C_r$ tolerance. (c) With $\pm 10\% L_m$ tolerance. (d) With $\pm 10\% L_b$ tolerance.

TABLE I
PARAMETERS OF (PSIM) SIMULATION SOFTWARE TOLERANCE SIMULATION IN THREE-PHASE *LLC*

Symbol	Parameter	Comments
L_{lk}	$0.61\ \mu H$	+10% for phase 1 and -10% for phase 3 in (a)
C_r	$82n\ F$	+10% for phase 1 and -10% for phase 3 in (b)
L_m	$7.8\ \mu H$	+10% for phase 1 and -10% for phase 3 in (c)
$L_b \to L_{eq1}$	$0.61\ \mu H$	+10% for phase 1 and -10% for phase 3 in (d)
f_s	$500\ kHz$	close to resonant frequency
R_{load}	$0.5\ \Omega$	approximately $220\ W$ output power

In order to concurrently display the tolerance impacts of leakage inductance and DCIArray reluctance in the simulation, we assume the system includes both leakage inductor and DCIArray, and the L_{eq1} of DCIArray is identical to the average leakage inductance, so the influence between DCIArray and leakage inductor on the resonant tank is equal. Four groups of parameter deviation will be tested with $\pm 10\% L_r$, $\pm 10\% C_r$, $\pm 10\% L_m$, and $\pm 10\% L_b$, respectively. Results are shown in Fig. 8(a)–(d) accordingly, with simulation parameters set as Table I.

Fig. 8(a) and (b) show a similar trend that the 10% tolerance of L_{lk} and C_r will have similar effects on current unbalancing, and they reacted similarly toward the increasing coupling coefficient, too; higher coupling coefficient will suppress the tolerance influence. Fig. 8(c) also clarified that magnetizing inductance variation has little impact on current balancing, and coupling has little effect on improvements for L_m tolerance. Moreover, Fig. 8(d) tells that the tolerance of DCIArray reluctance will also introduce unbalance to the system, but compared to L_{lk}, the increasing of coupling coefficient will not simply improve the sharing performance, a negative coupled DCIArray will display a better balance between $K = -0.3 \sim -0.1$; while positively coupled DCIArray will perform better when transfer from nonfull-stack to full-stack case.

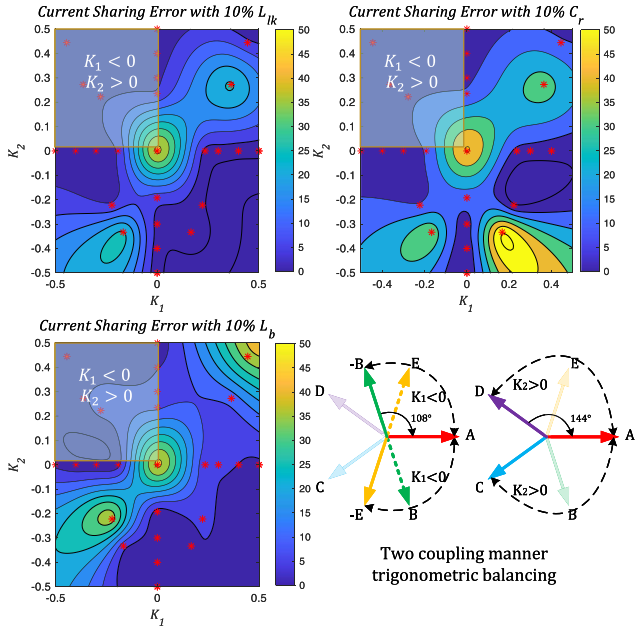

Fig. 9. Five-phase *LLC* current sharing error with tolerance and corresponding current coupling phasors.

To summarize, components tolerance will cause a similar unbalance current in uncoupled case, despite the possible extra error DCIArray may bring to the system, a coupled *LLC* converter will have better power distribution compared to the uncoupled case, and the increase of coupling coefficient will generally improve this sharing performance. For negative coupled, a lower coupling coefficient between $K = -(0.2 \sim 0.3)$ can suppress the sharing error from 40% to 5%; and a high positive coupling coefficient of $K = +(0.3 \sim 0.5)$ can take the sharing error down to 10%. Typically, a DCIArray will bring a balancing improvement by a factor of $4 \sim 8$, in a practical design, $K = \pm(0.3 \sim 0.5)$ can be considered as it is easy to implement.

When the theory is extended to a five, seven, or higher phase system, the sharing behavior will be more complicated, the reason is higher phase systems have more than one coupling coefficient. Take a five-phase system as an example, there will be two different coupling coefficients, according to (17), we have

$$\begin{cases} K_{12} = K_{23} = K_{34} = K_{45} = K_{51} \\ = \frac{N_1N_2+N_2N_3+N_3N_4+N_4N_5+N_5N_1}{N_1^2+N_2^2+N_3^2+N_4^2+N_5^2} = K_1 \\ K_{13} = K_{24} = K_{35} = K_{41} = K_{52} \\ = \frac{N_1N_3+N_3N_5+N_5N_2+N_2N_4+N_4N_1}{N_1^2+N_2^2+N_3^2+N_4^2+N_5^2} = K_2. \end{cases} \tag{21}$$

In order to investigate different coupling coefficients separately, we choose a nonfull-stack DCIArrays with only N_1, N_2, and N_3 as nonzero windings. Simulation results can be plotted in Fig. 9, with parameter settings in Table II. Converter will suffer from different kinds of current unbalance under different combinations of components tolerance, only in quadrant of $K_1 < 0$ and $K_2 > 0$, all current sharing error can be constrained in a low value.

TABLE II
PARAMETERS OF PSIM TOLERANCE SIMULATION IN FIVE-PHASE *LLC*

Symbol	Parameter	Comments
L_{lk}	$0.61\ \mu H$	+10% +5% -5% -10% for phase 1, 2, 4, 5 respectively in $\%10L_{lk}$ test
C_r	$82\ nF$	+10% +5% -5% -10% for phase 1, 2, 4, 5 respectively in $\%10C_r$ test
$L_b \to L_{eq1}$	0.61 uH	+10% +5% -5% -10% for phase 1, 2, 4, 5 respectively in $\%10L_b$ test
L_m	$7.8\ \mu H$	not included in variance analyze due to weak influence
f_s	$500\ kHz$	close to resonant frequency
R_{load}	$0.5\ \Omega$	approximately $220\ W$ output power

We can explain this behavior from the perspective of five-phase coupling phasor. When $K_1 < 0$ and $K_2 > 0$, phase currents are resisting each other in a triangle behavior, as trigonometric current can automatically tune the current phase angle to keep balance similar to [4]. Since DCIArray purposely related all phases in a symmetrical manner, no phase is left out of triangle balancing. Then, the unbalanced current caused by components tolerance can be suppressed.

Another conclusion for the multiphase DCIArray is the limit for coupling coefficient, in the full-stack case, the maximum coupling coefficient for an m phase converter can be calculated by following limit approximation:

$$\lim_{N_2,N_3,\ldots,N_m\to\infty} \frac{\sum N_pN_q}{\sum_{i=1}^{m} N_i^2} = \frac{m-2}{m-1}. \tag{22}$$

While in the nonfull-stack DCIArray, if there are n windings of the m-phase system with a turn number equal to zero, then this limit will be lower

$$\lim_{\substack{N_{n+1},N_{n+2},\ldots,N_m\to\infty \\ N_1=0,N_2=0,\ldots,N_n=0}} \frac{\sum N_pN_q}{\sum_{i=1}^{m} N_i^2} = \frac{m-1-n}{m-n}. \tag{23}$$

Evidently, as the turns ratio gets higher, the coupling coefficient will approach this asymptotic limit, so a nonfull-stack DCIArray with a low turns ratio is adequate for current sharing improvement.

E. Voltage Gain Characteristic and Control Architecture

In a multiphase discrete coupled *LLC* converter, coupled inductors will participate the resonant process and perform as a part of the resonant inductor, this was the combined effect of mutual inductance between all coupled phases.

For multiphase coupled converters, the equivalent inductance in different switching intervals is different, it should be sophisticated to determine its value. However, for multiphase *LLC* converters, since we can use the symmetrical component theory to decouple the multiphase system into a series of independent single-phase systems based on the current sequence, so the determination of the inductance value can become quite simple.

When we look back at the equivalent circuit for the multiphase *LLC* converter, the only tricky part is the independent unbalanced leakage inductances, which are always responsible for the unbalancing phase current. And we cannot use symmetrical component transformation to uncouple this unbalanced inductance. Take the three-phase system as an example, the leakage

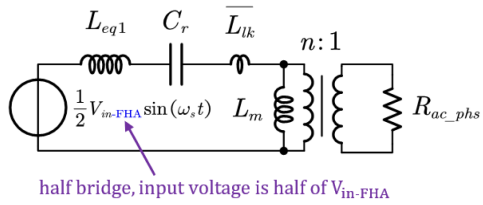

Fig. 10. Equivalent one-phase circuit for the m-phase *LLC* converter.

inductance after transformation can be expressed as

$$\mathbf{S}\begin{bmatrix} L_{\text{lk1}} & 0 & 0 \\ 0 & L_{\text{lk2}} & 0 \\ 0 & 0 & L_{\text{lk3}} \end{bmatrix}\mathbf{S^{-1}} = \begin{bmatrix} \overline{L_{\text{lk}}} & \Delta_1 & \Delta_2 \\ \Delta_2 & \overline{L_{\text{lk}}} & \Delta_1 \\ \Delta_1 & \Delta_2 & \overline{L_{\text{lk}}} \end{bmatrix}$$

$$\begin{cases} \overline{L_{\text{lk}}} &= \frac{1}{3}\left(L_{\text{lk1}} + L_{\text{lk2}} + L_{\text{lk3}}\right) \\ \Delta_1 &= \frac{1}{3}\left(L_{\text{lk1}} + \alpha^2 L_{\text{lk2}} + \alpha L_{\text{lk3}}\right) \\ \Delta_2 &= \frac{1}{3}\left(L_{\text{lk1}} + \alpha L_{\text{lk2}} + \alpha^2 L_{\text{lk3}}\right). \end{cases} \tag{24}$$

The unbalancing elements Δ_1 and Δ_2 account for the unbalancing current, but it is also miniature compared to the average leakage inductance $\overline{L_{\text{lk}}}$. So, the unbalance current will not seriously influence the voltage gain, then we can use average leakage inductance $\overline{L_{lk}}$ to substitute the leakage inductance in each phase, intended to obtain the equivalent one-phase *LLC* circuit.

Based on the FHA method, we first assume that the $V_{\text{in-FHA}}$ and $V_{\text{out-FHA}}$ represents the first harmonic wave effective value of the input voltage and output voltage of the phase resonant network, respectively. Then, we can draw the equivalent one-phase circuit for multiphase *LLC*, as shown in Fig. 10 as

$$\begin{cases} V_{\text{in-FHA}} &= \frac{2\sqrt{2}}{\pi} V_{\text{in}} \\ V_{\text{out-FHA}} &= \frac{2\sqrt{2}}{\pi} V_{\text{out}} \\ R_{\text{ac\_phs}} &= m \cdot \frac{8n^2}{\pi^2} R. \end{cases} \tag{25}$$

Then, the revised resonant frequency and corresponding voltage gain can be expressed as

$$f_r = \frac{1}{2\pi\sqrt{\left(L_{\text{eq 1}} + \overline{L_{\text{lk}}}\right) Cr}} \tag{26}$$

$$\begin{aligned} G_{\text{a c}} &= \frac{2nV_{\text{out-FHA}}}{V_{\text{in-FHA}}} \\ &= \left| \frac{j\omega L_m // R_{\text{ac\_phs}}}{j\omega\left(L_{\text{eq1}} + \overline{L_{\text{lk}}}\right) + 1/j\omega C_r + j\omega L_m // R_{\text{ac\_p h s}}} \right| \\ &= \frac{1}{\sqrt{\left[1 + \frac{1}{L_n} - \frac{1}{L_n f_n^2}\right]^2 + \left[Q_e\left(f_n - \frac{1}{f_n}\right)\right]^2}} \end{aligned}$$

$$\begin{cases} f_n = f_s / f_r \\ L_n = \frac{L_m}{L_{\text{eq1}} + \overline{L_{\text{lk}}}} \\ Q_e = \frac{\sqrt{\left(L_{\text{eq1}} + \overline{L_{\text{lk}}}\right)/C_r}}{R_{\text{ac\_phs}}} \end{cases} \tag{27}$$

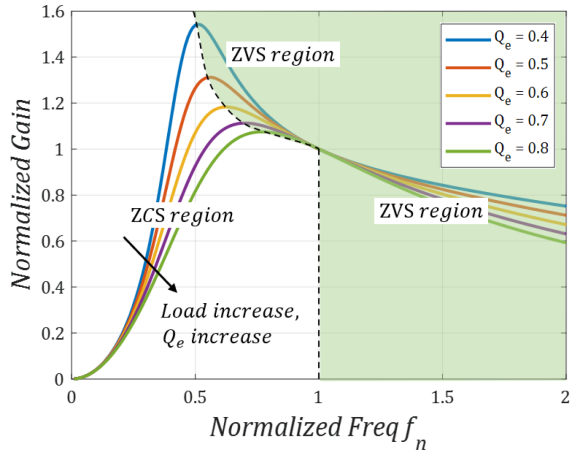

Fig. 11. Voltage gain curve for the m-phase *LLC* converter.

where n is the turns ratio between primary and secondary windings; L_n is defined as the inductance ratio of the transformer; and Q_e is the quality factor of the resonant tank.

This model is also valid for the m-phase *LLC* converter, the impact of a DCIArray on the voltage gain is equivalent to introducing a first-sequence inductance into the resonant tank. By designing the winding structure and unit inductance L_b of the DCIArray, we can perfectly control this first-sequence inductance, and further control the resonant tank parameters.

As soon as the voltage gain characteristic is determined, we can design a control system for the multiphase discrete coupled *LLC* converter. Since the voltage gain characteristic of the proposed converter is identical to a traditional single-phase *LLC* converter, the variable frequency control is still valid to adjust the output voltage, as shown in Fig. 12. The output voltage is sampled as feedback for frequency information, and the frequency range should be set within the ZVS range of Fig. 11. Then, fixing the phase shift angle of each phase gate turning-ON signal as $2\pi/m$ ($\phi_1 = 0$, $\phi_2 = 2\pi/m$ ... etc), the multiphase current will flow in a symmetrical manner.

III. Recommended Discrete Coupled Multiphase Inductor Design for Multiphase *LLC*

In this section, a recommended general coupling method for easier phase expansion is considered based on the phasor diagram. Then, a comparison between different coupling structures is implemented based on the sequence impedance diagram, both on three-phase and five-phase *LLC* converters.

A. General Recommended Coupling Method for Multiphase LLC Converter

Even though all possible coupled structure (with all possible winding turns) for the multiphase DCIArray is thoroughly discussed for theoretical needs, engineers do not want to apply too complex coupled structures into their converters. This means we should eliminate less-necessary windings and preserve the windings that really matter, especially for higher phases converters.

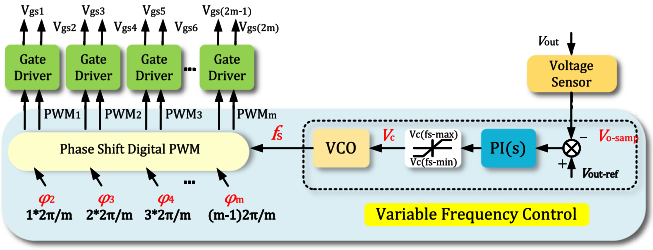

Fig. 12. Control architecture for the multiphase coupled *LLC* converter.

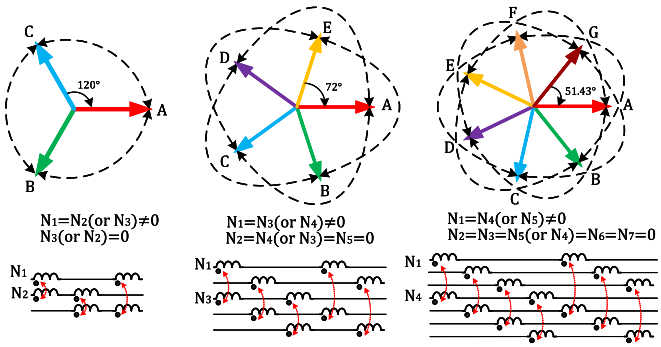

Fig. 13. General coupling structure based on the phasor diagram.

Based on the analysis in Section II, a nonfull-stack DCIArray with two different phases' windings per inductor to associate all phases may be more suitable for the real-world application. If we fix the N_1 winding turn, the only problem is to find which N_k makes the best balancing behavior.

Fig. 13 provides a feasible coupling structure. If each phase current is coupled with the other two largest phasor difference phases, then the current suppressing ability will be most significant, in this case, N_k can be chosen as $N_{(m+1)/2}$ or $N_{(m+3)/2}$. From the perspective of sequence impedance, it represents the circumstance that L_{eq1} is the smallest in all sequence impedance. This idea can also be reverified by the sequence impedance diagram, which will be discussed in detail in the next sections.

B. Recommended Coupling Structure for the Three-Phase Converter

The sequence impedance diagram for the nonfull-stack three-phase DCIArray can be seen from Fig. 6(b), since the three-phase system is highly symmetrical, letting N_1 to be zero is the same on other winding, so there is no need to redraw the diagram. From the diagram we know L_{eq0} is higher than L_{eq1} only when N_2 and N_3 have the same sign, which requires inductors to be positively coupled; while N_2 and N_3 has a different sign, L_{eq0} will be smaller than L_{eq1}, which means inductors are inversely coupled.

Although both coupled structures are capable of balancing the current in the three-phase system, it does not mean their balancing performance is the same on all frequency ranges. If both coupled structure provides the same value of first sequence impedance L_{eq1} for the resonant inductor, both coupled structure could provide a similar degree of balancing on the resonant frequency as analyzed in Section II-D.

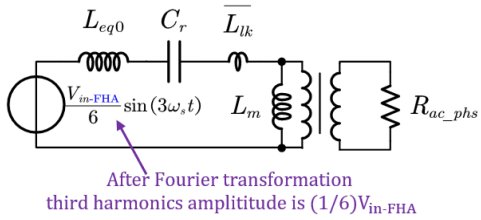

Fig. 14. Equivalent circuit for third harmonic in the three-phase *LLC* converter.

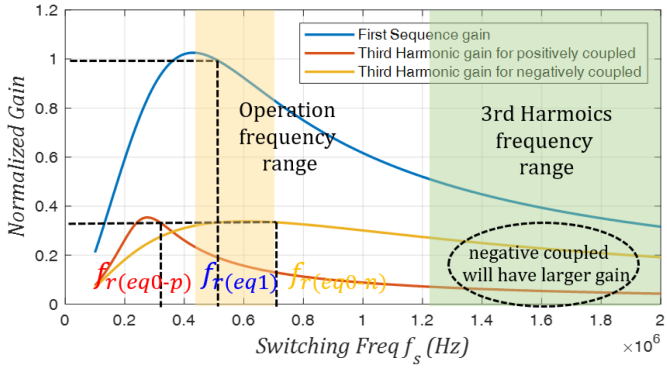

Fig. 15. Voltage gain for third harmonic under positive\negative coupling.

However, as the switching frequency deviates from the resonant point, especially when the switching frequency is higher than the resonant frequency, a positively coupled structure will generally provide better balancing due to high zero-sequence impedance.

$$f_{r(\text{eq0})} = \frac{1}{2\pi\sqrt{\left(L_{\text{eq0}} + \overline{L_{\text{lk}}}\right) Cr}}. \tag{28}$$

The aforementioned equation provides the resonant frequency of zero-sequence components, since the zero-sequence impedance L_{eq0} of the positively coupled *LLC* converter is always larger than negatively coupled case (with same L_{eq1}), the corresponding zero sequence resonant frequency $f_{r(\text{eq0-}p)}$ is always lower than $f_{r(\text{eq0-}n)}$. If the converter works above the resonant frequency, f_s will approach $f_{r(\text{eq0-}n)}$, which will deteriorate the balancing in the negatively coupled case.

Another special character for the three-phase discrete coupled *LLC* converter is the third harmonic that comes from the Fourier expansion of the interleaved input voltage. If the third harmonic of the square wave is not negligent, then there will be third harmonic sharing the path of zero sequence components, introducing third harmonic current to the system, as shown in the equivalent circuit for the third harmonic in Fig. 14. The voltage gain of the third harmonic can be calculated by (29). Then, we can plot the voltage gain of the third harmonic with the fundamental in a single diagram.

$$G_{\text{ac(3rd)}} = \frac{1}{3}\left|\frac{j\omega L_m // R_{\text{ac\_phs}}}{j\omega\left(L_{\text{eq0}} + \overline{L_{\text{lk}}}\right) + 1/j\omega C_r + j\omega L_m // R_{\text{ac\_phs}}}\right|. \tag{29}$$

Fig. 15 suggests that the third harmonic always has a higher gain in negatively coupled compared to the positively coupled case, this phenomenon can also be observed from the

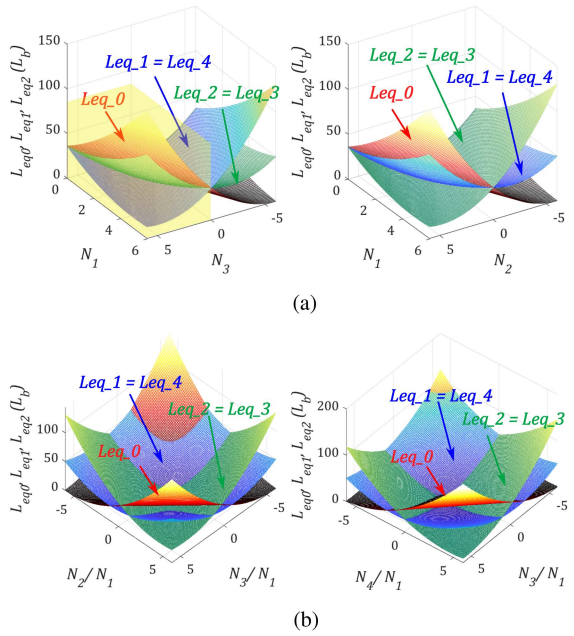

Fig. 16. Sequence impedance diagram for five-phase *LLC*. (a) With two non-zero windings. (b) With three non-zero windings.

experimental waveform in the next section, therefore, positively coupled DCIArray is more recommended for three-phase *LLC* converters, as it keeps a better sinusoidal behavior.

C. Recommended Five-Phase Discrete Coupled LLC Converter

Compared to three-phase *LLC*, five-phase *LLC* will introduce another pair of sequence impedances in a different value, according to the general sequence impedance equation in (17), the sequence impedance can be calculated as

$$\begin{cases} L_{\text{eq0}} = \left(\sum_{i=1}^{m} N_i\right)^2 L_b \\ L_{\text{eq1}} = L_{\text{eq4}} = [\sum_{i=1}^{m} N_i^2 + 0.618M_1 - 1.618M_2]L_b \\ L_{\text{eq2}} = L_{\text{eq3}} = [\sum_{i=1}^{m} N_i^2 - 1.618M_1 + 0.618M_2]L_b \\ M_1 = N_1N_2 + N_2N_3 + N_3N_4 + N_4N_5 + N_5N_1 \\ M_2 = N_1N_3 + N_3N_5 + N_5N_2 + N_2N_4 + N_4N_1. \end{cases} \tag{30}$$

If we choose a nonfull-stack DCIArray with only two nonzero windings per inductor, there will be only two valid cases, either each phase is coupled with the adjacent phase by interleaving 72°, or coupled with a nonadjacent phase of 144°. We can map these coupling structures as depicted in Fig. 16(a).

We can also plot the diagram of three nonzero windings DCIArray as Fig. 16(b), from all cases, we can find only in one circumstance, where the first sequence impedance has the least value among all sequence impedance, which is highlighted as a yellow region.

Combining the analysis in Section II-D, we can verify that higher sequence impedance will better suppress the corresponding sequence current, so the recommended coupling structure for five-phase *LLC* is each phase is only positively coupled with a 144° nonadjacent phase.

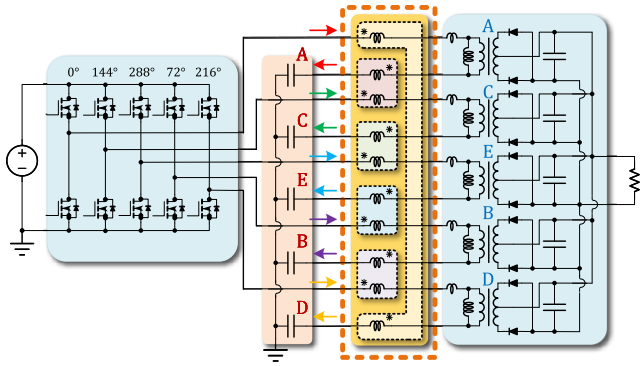

Fig. 17. Equivalent schematic of five-phase coupled *LLC* with DCIArray.

Fig. 17 is an equivalent circuit to insert the DCIArray into the resonant tank of the five-phase system. By modifying the DCIArray to a bidirectional routing method, each coupled inductor can be directly coupled with the adjacent phases. In order to maintain the 144° coupled structure, the switching order of each phase leg should be modified as well, as depicted in the schematic.

IV. Test Setup and Experiment Verification

In this section, the balancing performance of the proposed multiphase discrete coupled *LLC* converter is experimentally verified based on both three-phase and five-phase platforms, with different switching frequencies. Discussions on parasitic capacitance influence on the converter performance and possible improvement is proposed. Efficiency comparison and loss breakdown are exhibited with detailed measured parameters.

A. Testing Setup and Parameter Measurement

The testing bench setup for the three-phase and five-phase *LLC* converters are exhibited in Fig. 18, the prototype to verify the proposed balancing theory was built using a modular approach, the five-phase converter is formed by stacking up two three-phase modules with one phase channel disabled. The rectifiers for each phase are substituted by two active switches with a commercial synchronous rectifier control driver to improve the secondary side efficiency. The detailed part number and parameters for the prototype are presented in Table III.

As Fig. 18(a) shows, all ferrite cores are selected in commercially available types, and the geometrical arrangements of the inductor array did not affect the balancing behavior of discrete coupled *LLC* as long as the coil coupling schematic is maintained. The turns ratios for the tested three-phase nonfull-stack DCIArray are chosen to be 2:2 for positively coupled and 2:-2 for negatively coupled, respectively; five-phase DCIArray are chosen to be 2:1 with 144° coupling.

The measured inductance and capacitance values of the resonant tanks are taken down in Table IV; compared to the resonant capacitor, leakage inductance is much harder to control especially when the inductor is low and in the microhenry range. The inconsistency of wire-wound inductors is the major unbalancing

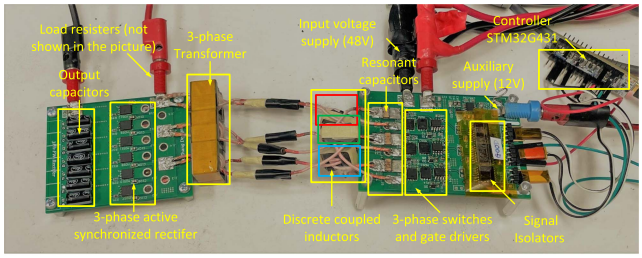

(a)

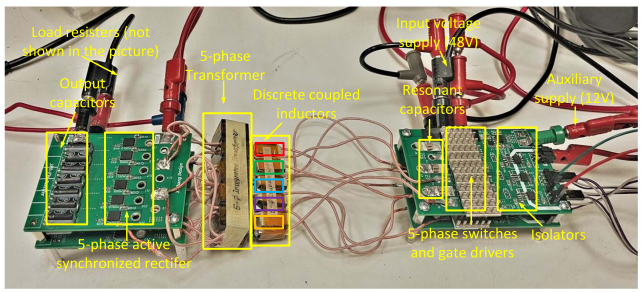

(b)

Fig. 18. Photograph of the proposed interleaved converter in the modular design. (a) Three-phase *LLC* testing setup. (b) Five-phase *LLC* testing setup.

TABLE III
HARDWARE PARAMETERS OF PROPOSED CONVERTER PROTOTYPES

Parameter	Value
Input voltage V_{in}	$36 \sim 54$ V
Output voltage V_{out}	12 V
Rated load resister	0.5 Ω
Transformer turns ratio n	2 : 1 : 1
Switching frequency f_s	$300 \sim 700\,kHz$
Primary Switches	ISC0802NLSATMA1
Secondary Switches	BSC040N10NS5
PWM micro-controller	STM32G474 or 431
Synchronous rectifier controller	NCP43080ADR2G
Transformer core	PQ20-3F3
Coupled inductor core	RM6S/I-3F3

TABLE IV
RESONANT TANK PARAMETERS OF PROPOSED CONVERTER PROTOTYPES

	Three-phase LLC converter					
Parameters	Phase A	Phase B	Phase C			Mean
$L_{lk}[\mu H]$	1.114	1.052	1.172			1.112
$C_r[nF]$	86	86	86			86
$L_m[\mu H]$	6.174	6.750	6.360			6.428
$L_{\text{ext}}[nH]$	702	728	709			713
$n_b^2 L_{b\text{-}pos}[nH]$	806	776	692			758
$n_b^2 L_{b\text{-}neg}[nH]$	263	274	251			263
$R_{ac\text{-wind}}[m\Omega]$	111	84	95			97
	Five-phase LLC converter					
Parameters	Phase A	Phase B	Phase C	Phase D	Phase E	Mean
$L_{lk}[\mu H]$	1.397	1.505	1.508	1.703	1.411	1.505
$C_r[nF]$	68	68	68	68	68	68
$L_m[\mu H]$	12.97	14.64	14.41	15.86	15.14	15.51
$L_b[nH]$	415	448	393	426	432	432

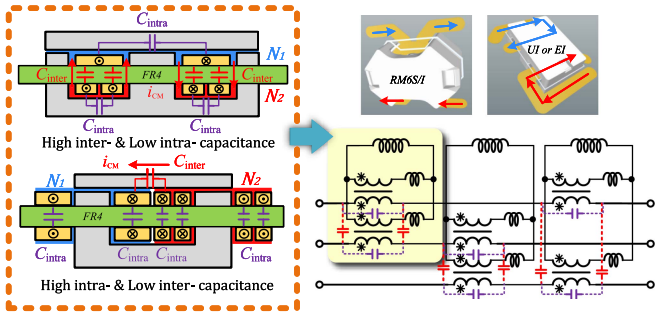

Fig. 19. Parasitic capacitance of two different discrete coupled inductors.

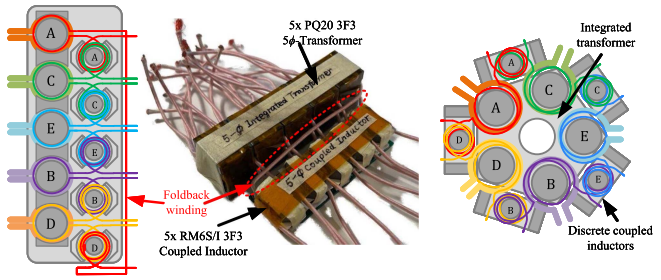

Fig. 20. Hand-made five-phase prototype and a possible ring-shaped pentagon magnetic integration method.

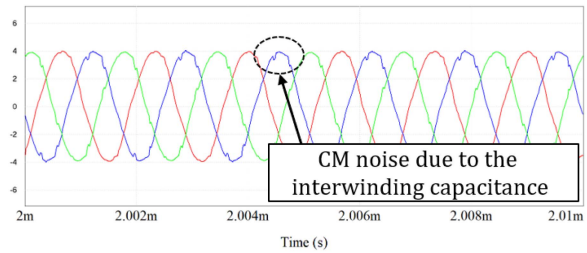

Fig. 21. Simulation with a 100-pF interwinding parasitic capacitor per inductor.

cause of multiphase dc\dc converters, so for higher power transformers, printed circuit board winding with planar integration should be considered since better components consistency and manufacturability can be confirmed.

B. Parasitic Capacitance and Magnetics Integration Problems

Parasitic capacitance is another concern that blocks the application for higher frequency *LLC* converters. According to [28] and [29], parasitic capacitance may cause transformer square-wave voltage distortion in light-load operation and high common-mode (CM) noise current in full-load operation. For the coupling structure proposed in the article, since the phase windings of coupled inductors overlap each other in the same leg of the core, the problem of parasitic capacitors will also arise in planar implementation. Fig. 19 is an illustration for a single inductor of nonfull-stack DCIArray, the estimated parasitic capacitance can be calculated using the equation provided by Saket et al. [29]. There are intrawinding capacitors and interwinding

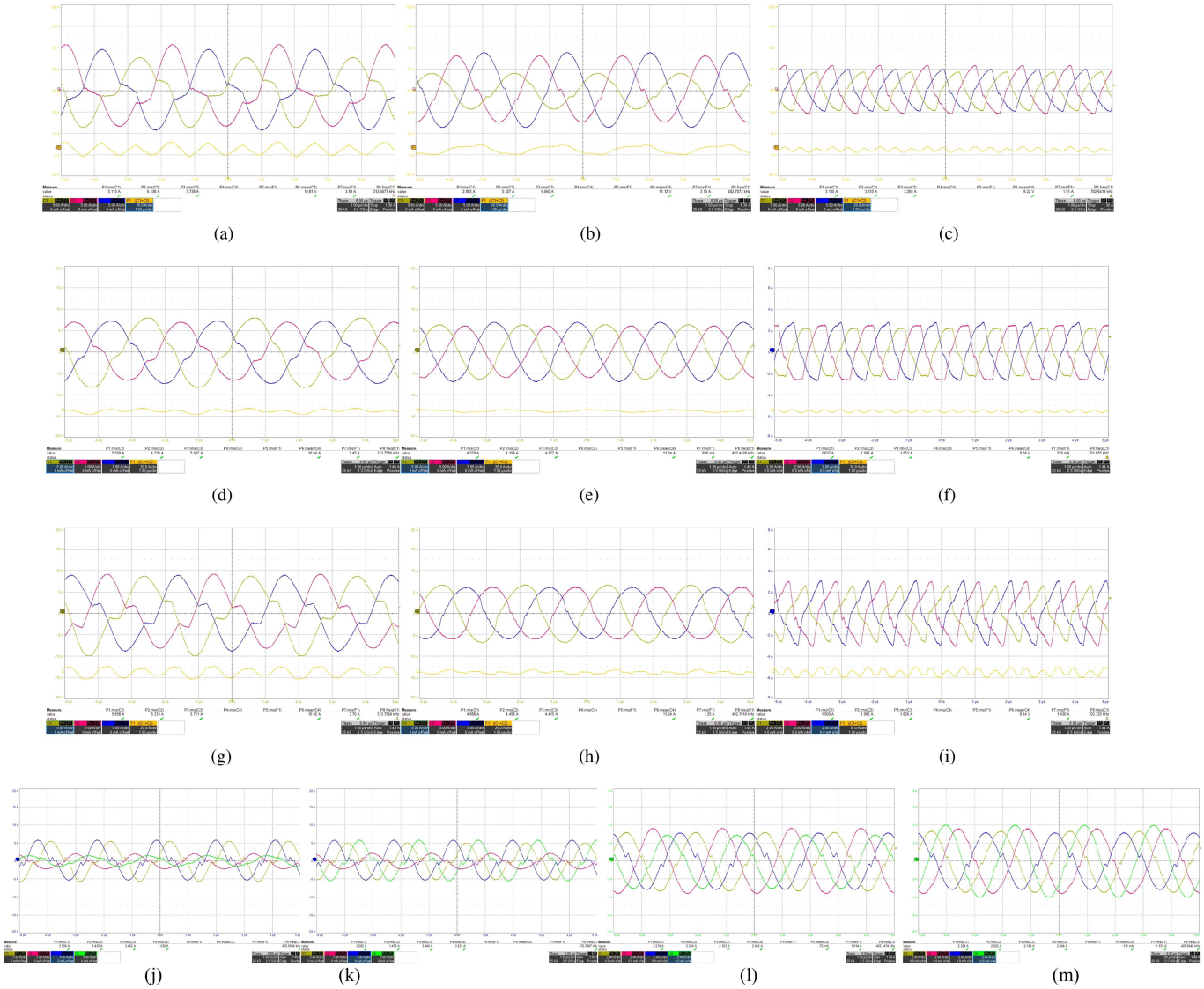

Fig. 22. Experimental waveform of three-phase and five-phase interleaved *LLC* converters for both uncoupled and coupled cases. (a) Uncoupled three-phase *LLC* with $f_s < f_r$. (b) Uncoupled three-phase *LLC* with $f_s = f_r$. (c) Uncoupled three-phase *LLC* with $f_s > f_r$. (d) Positively coupled three-phase *LLC* with $f_s < f_r$. (e) Positively coupled three-phase *LLC* with $f_s = f_r$. (f) Positively coupled three-phase *LLC* with $f_s > f_r$. (g) Negatively coupled three-phase *LLC* with $f_s < f_r$. (h) Negatively coupled three-phase *LLC* with $f_s = f_r$. (i) Negatively coupled three-phase *LLC* with $f_s > f_r$. (j) Uncoupled five-phase *LLC* (ABCE). (k) Uncoupled five-phase *LLC* (ABDE). (l) 144° coupled five-phase *LLC* (ABCE). (m) 144° coupled five-phase *LLC* (ABDE).

capacitors as shown in the figure.

$$C_{\text{intra}} = C_{\text{overlap}} = \frac{1}{3}\frac{\epsilon_0 \epsilon_r A_e}{d}$$
$$C_{\text{inter}} = C_{\text{adjacent}} = \frac{2(n-2)}{n^3}\epsilon_0 \frac{t}{W}\frac{A_t}{c} \tag{31}$$

where A_e represents the overlapping area between layers; ϵ_r is the FR4 permittivity; d is the distance between two layers; A_t represents the total area of turns; t is the thickness of copper; W is the width of traces; and c is the clearance between adjacent traces. When RM6 core is used in this letter, the estimated intrawinding capacitor per inductor will be only 2.86˜pF, which has nearly no impact on the converter. Only if the capacitance rises to about 100-pF level, then noticeable CM currents can be observed from full-load simulation as shown in Fig. 21. The simulation also suggests that intrawinding capacitance has low impact on resonant tanks.

Because the high interwinding capacitance is the main resource of CM noise, one possible solution is avoiding the overlapping of different phase currents, as shown in Fig. 19. This requires substituting center leg coupling to side leg coupling and keeping the same coupling manner, which results in the utilization of planar UI core and difficulties of full-stack coupling. However, these problems can be optimized as a higher power density is always a requirement. Fig. 20 provides the photograph of the five-phase magnetic prototype of the proposed converter, but because the discrete coupling method relies on the special arrangement of windings, a foldback winding is unavoidable in one phase, which may introduce a higher phase inductance, therefore, a ring shape planar core as referred in [34] is needed for further study in higher power integration.

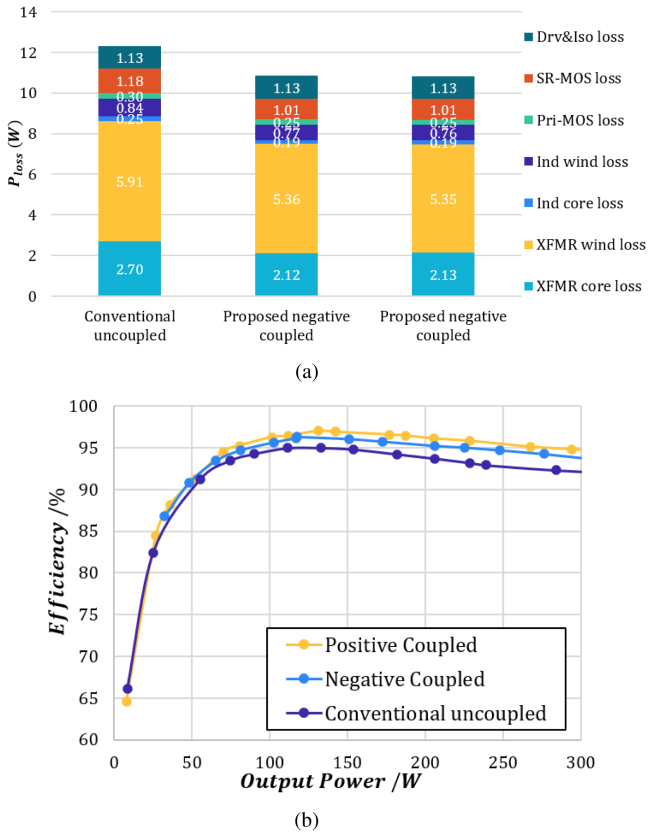

Fig. 23. Loss breakdown and measured efficiency for the proposed three-phase *LLC* converter. (a) Loss breakdown comparison of at the full-load condition. (b) Efficiency comparison of conventional and proposed method.

C. Experimental Results and Efficiency Comparison

Fig. 22(a)–(i) present the resonant currents of uncoupled, proposed positively coupled, and proposed negatively coupled three-phase converter. In order to perform a comparison under the same condition, the output power and switching frequencies for all corresponding coupled cases are fixed to be identical for the corresponding switching frequency. Using the determination from (26), the actual resonant frequency for the uncoupled case should be around 402 kHz, while for the positively and negatively coupled cases, it is around 397z and 394 kHz, respectively.

Fig. 22(b), (e), and (h) indicate a significant mismatch of currents in the uncoupled case when $f_s = f_r = 400$ kHz, while both positively and negatively coupled cases can provide good current sharing. Fig. 22(a), (d), and (g) show the different current manner when switching frequency is lower than the resonant frequency and equals to 314 kHz, where positively coupled can maintain a better sinusoidal and low rms current; Fig. 22(c), (f), and (i) provide the current distortion when f_s=700 kHz is above the resonant point, the waveforms are consistent to the third harmonic analysis in Section III-B, where the negatively coupled case will have the largest zero-sequence current compared to two other cases due to higher third harmonic gain and low L_{eq0} (zero-sequence currents are obtained from the real-time math function of the oscilloscope, by summarizing three-phase currents). Overall, different discrete coupled inductors are both providing a noticeable current balancing in all frequency ranges.

Fig. 22(h)–(j) also provide the current balancing ability of the five-phase discrete coupled *LLC* converter. The uncoupled five-phase converter encountered a worst current sharing case as referred in [35], where only three phases share the load power. After introducing a nonfull-stack coupled array with 144° coupling, the current sharing gets much better, which verified the theory proposed in this article.

1) Magnetics Power Losses Estimation: The current and flux in *LLC* converters follow perfect sinusoidal behavior and no dc bais, so the magnetic loss per unit volume of the chosen core shape can be computed by the conventional Steinmetz equation given by [10]

$$P_{\text{core}} = k_{Fe} \Delta B^{\beta} A_e l_e \tag{32}$$

where k_{Fe} is the Steinmetz constants fitting from the manufacturer's published data, ΔB is the ac flux density, typical values of β ranges from 2.6 to 2.8, and A_e and l_e are effective area and length of the selected cores.

In *LLC* converters, the ac flux ΔB is two times the maximum flux in the core, we can directly use the measured inductance information to calculate the ac flux

$$\Delta B = 2B_{pk} = 2\frac{I_{Lr\text{-}pk}}{NA_e} \tag{33}$$

where $I_{Lr\text{-}pk}$ is the peak value of each phase's current, L is equal to L_m in transformers calculation or L_b in externally coupled inductors calculation, and N should be correspondingly equal to N_p of the transformer or N_{Lb} of the inductor.

As for conduction losses in the cores, we can directly use the measure ac resisters value in Table IV

$$P_{\text{wind}} = R_{\text{ac-wind}} I^2_{Lr\text{-rms}}. \tag{34}$$

By substituting the full-load current information of the converter in Fig. 22(b), (e), and (h) into (32)–(34), the estimated losses from the magnetics devices can be calculated.

2) Switches Devices Power Losses Estimation: If the ZVS operation can be guaranteed, the turn-ON losses of all switches can be ignored. Besides, the utilization of synchronous rectifier controllers can decrease the losses in SR MOSFETs, then the switches losses can be calculated as

$$\begin{aligned} P_{\text{pri-MOS}} &= R_{ds\text{-pri}} I^2_{Lr\text{-rms}} \\ P_{\text{sec-MOS}} &= R_{ds\text{-SR}} \left(nI_{Lr\text{-rms}}\right)^2. \end{aligned} \tag{35}$$

Then, the estimated losses breakdown can be plotted in Fig. 23(a), which shows the major part of power losses consumed on the transformer and inductor windings. Even though discrete coupled converters introduce extra inductor losses, the benefit of current sharing on other losses exceeds the drawbacks it brings. To be specific, the balanced resonant currents will decrease the conduction losses in both transformer windings and active switches, since the power distribution is more even in the ferrite, the core losses in magnetics will decrease, too. For active switches, coupled *LLC* converters will go through lower uneven stresses, which also decreases the switches' losses. Overall, the proposed discrete coupled structure may increase the efficiency to about 1–2% and increase more as the power gets higher.

TABLE V
COMPARISON OF CURRENT SHARING SOLUTIONS IN OTHER LITERATURES

Converter	Interleaved operation ability	Cost	Complexity of control	Auxiliary devices
this work	Yes (Expandable)	Low	(Low) Fixed phase shift+frequency control	DCIArray
[4]	Yes (3ϕ LLC only)	High	(High) Trigonometric Phase shift	Phase current sampling
[16], [17]	Yes (Expandable)	High	(High) SCC compensation control	Extra SCC per phase
[6], [37]	Yes (Expandable)	High	(High) Phase shift for regulation circuit	Regulation Buck or DAB
[13], [21]	Yes (3ϕ LLC only)	Low	(Low) Fixed phase shift+frequency control	No
[35]	Yes (5ϕ LLC only)	Low	(Low) Fixed phase shift+frequency control	Bulk CLC filter
[31], [33]	No	Low	(Low) Frequency control	Common resonant Ind or Cap
[25], [1]	Yes (Expandable)	Low	(Low) Fixed phase shift+frequency control	ICBT/ balancing transformer
[36]	Yes (3ϕ LLC only)	Low	(Low) Fixed phase shift+frequency control	ICRI
[40]	No	High	(Low) Frequency control	Secondary wind grouping
[9], [8]	Yes (Expandable)	High	(High) Balancing phase shift control	VCVS windings

Fig. 23(b) shows the measured efficiency curves of the converter at different output power that generally matches the loss estimation. The full-load condition is designed to be 220 W, with an efficiency of 96.01% on positively coupled, 95.68% on negatively coupled, and 93.73% on the uncoupled case. It can be seen that the efficiency of the converter is the highest when it works approaching 150 W. All cases perform similar efficiency at very low power within 100 W, but positively and negatively coupled converters show similar efficiency even to rated power, both higher than the conventional uncoupled cases due to better current sharing.

A comparative study was also completed to emphasize the merits of the proposed multiphase discrete coupled *LLC* converter. In Table V, a summary of the interleaving ability, cost, control complexity, and auxiliary device requirement is shown for the DICArray compared to other recently proposed *LLC* converters. As seen from Table V, most current sharing techniques cannot reconcile the dilemma of interleaved operation and less control complexity and low cost; when both requirements are taken into account, the balancing ability is always constrained in a three-phase system. While proposed solution achieved a highly expandable and easy integration of magnetic-based current balancing with simple fixed phase shift control. Therefore, we can conclude that DCIArray is a promising method for the multiphase *LLC* converter.

V. CONCLUSION

This article presents an extendable and flexible coupling structure that inherently balances the current in multiphase interleaved *LLC* converters, with an analytical method using the generalized symmetrical components theory to better assess, design, and improve the overall coupling performance. The performance of the proposed method is validated through experiments both on three-phase *LLC* converters and five-phase converters. All efforts in this article can draw the following conclusion.

1) Current magnetic-based balancing techniques for *LLC* converters can find a general explanation and special treatment using the proposed modeling approach. The sequence impedance theory is helpful in identifying the unbalance current in multiphase *LLC* converters.
2) Proposed coupling structure can maintain the benefit of interleave operation as well as good current sharing performance, which is a promising solution for the high-power dc/dc power delivery system.
3) Magnetics integration and high-precise model-based control are required for future investigation, there are still many remaining problems to solve in the multiphase *LLC* converter to be a practical industrial application.

REFERENCES

[1] U. Ahmad, H. Cha, and N. Naseem, "Integrated current balancing transformer based input-parallel output-parallel LLC resonant converter modules," *IEEE Trans. Power Electron.*, vol. 36, no. 5, pp. 5278–5289, May 2021.
[2] M. H. Ahmed, C. Fei, F. C. Lee, and Q. Li, "48-V voltage regulator module with PCB winding matrix transformer for future data centers," *IEEE Trans. Ind. Electron.*, vol. 64, no. 12, pp. 9302–9310, Dec. 2017.
[3] A. Arafat, S. Choi, and J. Baek, "Open-phase fault detection of a five-phase permanent magnet assisted synchronous reluctance motor based on symmetrical components theory," *IEEE Trans. Ind. Electron.*, vol. 64, no. 8, pp. 6465–6474, Aug. 2017.
[4] S. A. Arshadi, M. Ordonez, W. Eberle, M. A. Saket, M. Craciun, and C. Botting, "Unbalanced three-phase LLC resonant converters: Analysis and trigonometric current balancing," *IEEE Trans. Power Electron.*, vol. 34, no. 3, pp. 2025–2038, Mar. 2019.
[5] R. Betz and T. Summers, "Introduction to symmetrical components and their use in STATCOM applications," Univ. Newcastle, Callaghan, NSW, Australia, Tech. Rep., Mar. 2005, doi: 10.13140/RG.2.1.2384.3043.
[6] H. Chen, X. Wu, and S. Shao, "A current-sharing method for interleaved high-frequency LLC converter with partial energy processing," *IEEE Trans. Ind. Electron.*, vol. 67, no. 2, pp. 1498–1507, Feb. 2020.
[7] M. Chen and C. R. Sullivan, "Unified models for coupled inductors applied to multiphase PWM converters," *IEEE Trans. Power Electron.*, vol. 36, no. 12, pp. 14155–14174, Dec. 2021.
[8] H. Dong, X. Xie, S. Xu, and H. Yu, "A novel current sharing scheme for two-phase interleaved LLC converter based on virtual controllable voltage sources," *IEEE Trans. Power Electron.*, vol. 37, no. 2, pp. 1210–1216, Feb. 2022.
[9] H. Dong, X. Xie, H. Yu, and D. Yu, "Improved multiphase interleaved LLC resonant converter with virtual controllable voltage sources," *IEEE J. Emerg. Sel. Topics Power Electron.*, vol. 11, no. 1, pp. 806–817, Feb. 2023.
[10] R. W. Erickson and D. Maksimović, "Basic magnetics theory," in *Fundamentals of Power Electronics*, R. W. Erickson and D. Maksimović, Eds. Cham, Switzerland: Springer, 2020, pp. 409–458.
[11] X. Fang, "Analysis and design optimization of resonant DC-DC converters," Ph.D. dissertation, Elect. Eng. Comput. Sci. Dept., Univ. Central Florida, Orlando, FL, USA, 2012.
[12] C. Fei, "Optimization of LLC resonant converters: State-trajectory control and PCB based magnetics," Ph.D. dissertation, Dept. Elec. Eng., Virginia Tech., Blacksburg, VA, USA, 2018.
[13] C. Fei, R. Gadelrab, Q. Li, and F. C. Lee, "High-frequency three-phase interleaved LLC resonant converter with GaN devices and integrated planar magnetics," *IEEE J. Emerg. Sel. Topics Power Electron.*, vol. 7, no. 2, pp. 653–663, Jun. 2019.
[14] Z. Guo, C. Wang, S. Lin, L. Yang, and X. Lu, "Multi-parallel and flexible expansion of single-switch WPT inverter by magnetic integration," *IEEE Trans. Power Electron.*, vol. 38, no. 3, pp. 4167–4180, Mar. 2023.
[15] Z. Hu, Y.-F. Liu, and P. C. Sen, "Bang-bang charge control for LLC resonant converters," *IEEE Trans. Power Electron.*, vol. 30, no. 2, pp. 1093–1108, Feb. 2015.
[16] Z. Hu, Y. Qiu, Y.-F. Liu, and P. C. Sen, "A control strategy and design method for interleaved LLC converters operating at variable switching frequency," *IEEE Trans. Power Electron.*, vol. 29, no. 8, pp. 4426–4437, Aug. 2014.

[17] Z. Hu, Y. Qiu, L. Wang, and Y.-F. Liu, "An interleaved LLC resonant converter operating at constant switching frequency," *IEEE Trans. Power Electron.*, vol. 29, no. 6, pp. 2931–2943, Jun. 2014.
[18] Z. Hu, L. Wang, H. Wang, Y.-F. Liu, and P. C. Sen, "An accurate design algorithm for LLC resonant converters—Part I," *IEEE Trans. Power Electron.*, vol. 31, no. 8, pp. 5435–5447, Aug. 2016.
[19] F. Jin, A. Nabih, Q. Li, and F. C. Lee, "A three phase CLLC converter with improved planar integrated transformer for fast charger applications," in *Proc. IEEE 4th Int. Conf. DC Microgrids*, 2021, pp. 1–5.
[20] F. C. Lee, Q. Li, and A. Nabih, "High frequency resonant converters: An overview on the magnetic design and control methods," *IEEE J. Emerg. Sel. Topics Power Electron.*, vol. 9, no. 1, pp. 11–23, Feb. 2021.
[21] B. Li, Q. Li, and F. C. Lee, "Phase shading for light load efficiency improve in three-phase resonant converter with integrated PCB winding magnetics," in *Proc. 10th Int. Conf. Power Electron. ECCE Asia*, 2019, pp. 2362–2367.
[22] Z. Liu, Z. Zheng, L. Xu, K. Wang, and Y. Li, "Current balance control for symmetrical multiphase inverters," *IEEE Trans. Power Electron.*, vol. 31, no. 6, pp. 4005–4012, Jun. 2016.
[23] K. Murata and F. Kurokawa, "An interleaved PFM LLC resonant converter with phase-shift compensation," *IEEE Trans. Power Electron.*, vol. 31, no. 3, pp. 2264–2272, Mar. 2016.
[24] N. Naseem and H. Cha, "Automatic mitigation of current imbalance for m-phase interleaved LLC resonant converter," *IEEE Trans. Power Electron.*, vol. 37, no. 9, pp. 10122–10127, Sep. 2022.
[25] M. Noah et al., "A current sharing method utilizing single balancing transformer for a multiphase LLC resonant converter with integrated magnetics," *IEEE J. Emerg. Sel. Topics Power Electron.*, vol. 6, no. 2, pp. 977–992, Jun. 2018.
[26] M. Noah, J. Imaoka, Y. Ishikura, K. Umetani, and M. Yamamoto, "Review of current balance mechanism in multiphase LLC resonant converters," in *Proc. IEEE 27th Int. Symp. Ind. Electron.*, 2018, pp. 1030–1036.
[27] E. Orietti, P. Mattavelli, G. Spiazzi, C. Adragna, and G. Gattavari, "Two-phase interleaved LLC resonant converter with current-controlled inductor," in *Proc. Braz. Power Electron. Conf.*, 2009, pp. 298–304.
[28] M. Pahlevaninezhad, D. Hamza, and P. K. Jain, "An improved layout strategy for common-mode EMI suppression applicable to high-frequency planar transformers in high-power DC/DC converters used for electric vehicles," *IEEE Trans. Power Electron.*, vol. 29, no. 3, pp. 1211–1228, Mar. 2014.
[29] M. A. Saket, N. Shafiei, and M. Ordonez, "LLC converters with planar transformers: Issues and mitigation," *IEEE Trans. Power Electron.*, vol. 32, no. 6, pp. 4524–4542, Jun. 2017.
[30] M. Sato, R. Takiguchi, J. Imaoka, and M. Shoyama, "A novel secondary PWM-controlled interleaved LLC resonant converter for load current sharing," in *Proc. IEEE 8th Int. Power Electron. Motion Control Conf.*, 2016, pp. 2276–2280.
[31] Z. Sun et al., "A unified common inductor and common capacitor current sharing method for multiphase LLC converter," *IEEE Trans. Power Electron.*, vol. 37, no. 10, pp. 12182–12196, Oct. 2022.
[32] H. Wang et al., "An algorithm to analyze circulating current for multi-phase resonant converter," in *Proc. IEEE Appl. Power Electron. Conf. Expo.*, 2016, pp. 899–906.
[33] H. Wang, Y. Chen, and Y.-F. Liu, "A passive-impedance-matching technology to achieve automatic current sharing for a multiphase resonant converter," *IEEE Trans. Power Electron.*, vol. 32, no. 12, pp. 9191–9209, Dec. 2017.
[34] J. Wang, J. Hu, W. Pei, Z. Yang, J. Zhuang, and X. Zhang, "In-depth design and multi-objective optimization of an integrated transformer for five-phase LLC resonant converters," *IEEE Trans. Power Electron.*, vol. 37, no. 11, pp. 13538–13553, Nov. 2022.
[35] J. Wang, W. Pei, J. Hu, S. Zhao, and J. Zhuang, "Five-phase LLC resonant DC/DC converter utilizing CLC filter for current sharing," *IEEE Trans. Ind. Electron.*, vol. 70, no. 9, pp. 8634–8644, Sep. 2023.
[36] L. Wang, D. Zhang, J. Duan, and Y. Hao, "High-frequency 12 V regulated LLC bus converter with integrated multi-phase inverse coupled resonant inductor," *IEEE Trans. Power Electron.*, vol. 38, no. 5, pp. 5742–5762, May 2023.
[37] M. Wang, X. Zha, S. Pan, J. Gong, and W. Lin, "A current-sharing method for interleaved high-frequency LLC converter with partial energy phase shift regulation," *IEEE J. Emerg. Sel. Topics Power Electron.*, vol. 10, no. 1, pp. 760–772, Feb. 2022.
[38] Y. Wei and A. Mantooth, "A family of LLC converters with magnetic control," in *Proc. IEEE Appl. Power Electron. Conf. Expo.*, 2021, pp. 783–789.
[39] B. Yang, "Topology investigation for front end DC/DC power conversion for distributed power system," Ph.D. dissertation, Dept. Elec. Eng., Virginia Tech., Blacksburg, VA, USA, Sep. 2003.
[40] Y. Yang, J. Yao, H. Li, and J. Zhao, "A novel current sharing method by grouping transformer's secondary windings for a multiphase LLC resonant converter," *IEEE Trans. Power Electron.*, vol. 35, no. 5, pp. 4877–4890, May 2020.

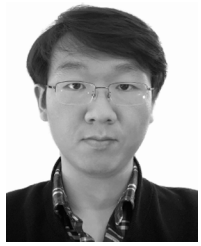

Xiang Zhang received the B.Sc. degree in electrical engineering from Wuhan University, Wuhan, China, in 2020. He is currently working toward the M.A.Sc. degree in electrical engineering with Queens's University, Kingston, ON, Canada.

He is a part-time Engineer with SPARQ SYSTEM INC, Kingston. His research interests include high power density resonant converters, magnetic integration in power converters, and dynamic modeling of power electronics.

Mr. Zhang was the recipient of Mitacs Globalink graduate fellowship.

Shangzhi Pan (Senior Member, IEEE) received the B.Sc. and M.Sc. degrees from Zhejiang University, Hangzhou, China, in 1998 and 2001, respectively, and the Ph.D. degree from Queen's University, Kingston, ON, Canada, in 2008, all in electrical engineering.

He was a Senior Research Engineer with Queen's University from 2008 to 2013. He worked as the VP of research and development with SPARQ Systems, a Queen's Spun-off PV microinverter company, since 2010. He joined the College of Electrical Engineering, Wuhan University, Wuhan, China, in 2018, where he is currently a Professor. He has also been an Adjunct Faculty with the Queen's Center of Energy and Power Electronics Applied Research Laboratory (ePOWER) since 2014. His research interests include digital control techniques for power converters, grid-connected inverters, voltage regulators for computing systems, power converters for renewable energy sources, and power converters for electric vehicles.

Praveen Jain (Fellow IEEE) received the M.A.Sc. and Ph.D. degrees in electrical engineering from the University of Toronto, Toronto, ON, Canada, in 1984 and 1987, respectively.

He played a key role in the design and development of high-frequency power conversion equipment for the International Space Station, Canadian Astronautics, in the late 1980s. He made pioneering contributions in introducing resonant power conversion technology in telecommunications during his work with Nortel in the 1990s. Over the last 35 years, he has made sustained contributions to the theory and practice of power electronics through his considerable consulting work with industry. He is the founder of two successful start-up companies, CHiL Semiconductor in the area of digital power controller (acquired by International Rectifier), and SPARQ Systems in the area of photovoltaic microinverters and energy storage. He is currently a Professor of electrical and computer engineering, Tier 1 Canada Research Chair in Power Electronics, and the Director of the Centre for Energy and Power Electronics Research with Queen's University, Kingston, ON, Canada. He has supervised and guided more than 100 graduate students, postdoctoral fellows, and power electronics engineers. He has authored and co-authored more than 600 papers and holds more than 100 patents.

Dr. Jain was the recipient of the 2021 IEEE Medal in Power Engineering, the 2017 IEEE Canada Electric Power Medal, the 2011 IEEE William Newell Power Electronics Award, and the 2004 Engineering Medal of the Ontario Professional Engineers. He is a Fellow of the Royal Society of Canada, the Engineering Institute of Canada, and the Canadian Academy of Engineering.